UNIVERSITY OF SOUTHAMPTON

Machine learning application to aircraft gust reconstruction

Supervisor: Prof. Andrea Da Ronch

Student: Peidong WU

Dissertation for the degree of MSc Computational Engineering and Design

Faculty of Engineering and Physical Sciences

Oct_2022

'This thesis was submitted for examination in month, year. It does not necessarily represent the final form of the thesis as deposited in the University after examination.'

I, (your name) declare that this thesis and the work presented in it are my own and has been generated by me as the result of my own original research.
I confirm that:
1. This work was done wholly or mainly while in candidature for a degree at this University;
2. Where any part of this thesis has previously been submitted for any other qualification at this University or any other institution, this has been clearly stated;
3. Where I have consulted the published work of others, this is always clearly attributed; 4. Where I have quoted from the work of others, the source is always given. With the exception of such quotations, this thesis is entirely my own work;
5. I have acknowledged all main sources of help;
6. Where the thesis is based on work done by myself jointly with others, I have made clear exactly what was done by others and what I have contributed myself;
7. Either none of this work has been published before submission, or parts of this work have been published as: [please list references below]:

ABSTRACT

This report examines the Master's research project Machine learning application to aircraft gust reconstruction. This project focuses on the reconstruction of gusts loaded on aircraft using machine learning techniques. Through the gust response of the aircraft, the dynamics and structure of the aircraft, the aerodynamic system and the control system are integrated to reconstruct the structure of the atmospheric motion (such as the profile velocity) of the gust. Initially, in this report, in the first part of the report, the basic theory required for gust reconstruction is introduced, including the study of the causes of gusts, the types of loads on the aircraft, and the gusts based on the airworthiness of the aircraft. Loading standards, the theoretical methods of analysing gust loads, and Aerodynamic and aeroelastic models are now necessary to perform load analysis in order to meet the standards. Then, the two mainstream gust load reconstruction methods are introduced, and the scope of their use and their respective advantages and disadvantages are described. After that, machine learning is introduced, some applications of machine learning in aircraft design are listed, and the application methods that appear in the application are introduced. After that, the research goals and objectives of the project are introduced. The third section describes the research methodology used in this research project, including Aerodynamic and aeroelastic models and selected machine learning algorithms for the reconstruction of gusts. The fourth section presents the results of the gust reconstruction and discusses what happened in the experiments, and explains the reasons for the problems in the experimental results. The fifth section discusses the remaining problems with the application of machine learning to the gust reconstruction problem and proposes possible solutions to these problems based on this study. The last section summarises the entire research project.

Contents

List of Figures

Nomenclature

1, INTRODUCTION

Turbulence or gusts will place dynamic loads on the aircraft structure, and gusts will inevitably be encountered by the aircraft during its service life. Severe turbulence may affect the static design strength of the aircraft, while relatively mild turbulence can also cause fatigue damage to the aircraft structure, so these loads need to be estimated during the design phase of the aircraft.

Gusts started from 20. In fact, half leaves were studied, and the first gust load specification was established in 1934. In 1957, the revised gust load formula was incorporated into Part 4B-3 of the U.S. Civil Aviation Regulations, marking the first step toward developing more advanced techniques for analysing aircraft dynamic responses.

In the 1940s and 1950s, the discrete gust method was used to simulate the velocity profile of wind gusts. Although this method does not return true air turbulence, it provides a model for evaluating normal acceleration in future designs. In the 1960s and 1970s, spectroscopic techniques were developed to design aircraft for gusting winds. For many years, gust predictions have been mainly done through inverse methods and optimisation methods.

Next, the theoretical background and related research of this report will be introduced in detail.

1.1, Aircraft load

In order to determine the fatigue capability that the aircraft structure needs to be able to withstand during the entire service life or the design strength required by the aircraft, it is necessary to evaluate the loads that the aircraft may bear. Loads are mainly divided into two categories for analysis, which are static and dynamic loads and fatigue loads. In order to prevent permanent deformation or failure of the aircraft structure, the aircraft structure must be able to withstand static and dynamic loads, which leads to the vast majority of calculations about static and dynamic loads. Although the fatigue load is much smaller than the static and dynamic loads, because the fatigue load will be repeatedly loaded, the aircraft structure must also be able to withstand it without failure due to it. Wing shear, bending moments and torques are of paramount importance when evaluating loads if a more detailed design is not required. But if detailed design is required, fuselage or tail shear forces, inertial loads, aerodynamic loads and external loads such as engine thrust and internal stresses also need to be considered. Because it is necessary to ensure that the aircraft can be put into service until the end of its service life, it is necessary to start from the detailed design stage of the aircraft to use the design strength of each component to remove the load and to check the stress stage to confirm that each component meets the previously determined design strength. . Ultimately, the structural engineer still needs to certify that the aircraft is strong enough to withstand the loading conditions specified in the airworthiness requirements. Flight and ground accidents resulting from actions such as atmospheric turbulence, descent speed landings, and ground manoeuvres are the most important sources of loads in an aircraft's life cycle.

In any case, the load consists of inertial loads, the distributed mass of the aircraft, and imposed load conditions such as wind gusts, control surface displacements, and landing gear reactions. The load cases are mainly divided into four sections: gust and turbulence loads involve dynamic aeroelasticity studies, which are formed by the full interaction of inertial forces with aerodynamic and elastic forces. Ground manoeuvring loads resulting from the interaction of elastic and inertial forces are classified as part of

the vibration study. In contrast, the discipline of stability and control requires the study of aircraft dynamic loads, which result from the interaction of inertial and aerodynamic forces. Finally, the subject of static aeroelasticity includes manoeuvring loads, which result from the interaction of aerodynamic and elastic forces. These four types of loads can be divided into two categories: bookcase and rational [1]. Bookcase refers to the relative artificial state of the aircraft, that is when inertial loads and external loads are balanced. This category is mainly used to study the state of aircraft balance manoeuvres but also includes some ground manoeuvres. Rational, on the other hand, is a more realistic condition where aircraft dynamics are studied through modelling and simulation. Rational applies to wind gusts or turbulence events as well as dynamic and ground manoeuvres and determines the maximum and ultimate loads expected in the use of the aircraft to ensure that the aircraft structure can withstand the loads during service without incurring deleterious permanent deformation.

1.2, Gust loads requirement

1.2.1, History

A gust load specification was first established in 1934 [1], based on the aircraft encountering a sharp-edged or step-function gust of intensity U; then, under the assumptions of quasi-steady aerodynamics and non-vertical motion of the aircraft, the incremental lift is given by

$$\Delta L = a\left(\frac{\rho V^2}{2}\right)S\left(\frac{U}{V}\right) \tag{1}$$

where a is the slope of the lift curve per radian and U/V is the increased angle of attack due to wind gusts and it is measured in radians. The acceleration increment can be obtained by Newton's second law

$$\Delta n = \frac{1/2\,\rho a V U}{W/S} \tag{2}$$

In 1941, to account for unsteady aerodynamic effects due to gust penetration and vertical response motion of the aircraft found in NACA studies of the Lockheed XC-35 aircraft [1], a moderation factor was introduced into the sharp-edged gust equation. K. When the mitigation factor K is first introduced, the mitigation silver varies with wing loading. On the other hand, because the thinking at the time was that gust velocity increased linearly with distance, the mitigation factor could be up to 10 chord lengths. In 1946, in order to meet the gust design value depending on the flight speed, the gust design requirement based on the V-n diagram was introduced, as shown in figure 1. Transient effects on flexible aircraft entered the equation in 1951. The dimensionless parameter μ_g not only considers the wing load but also includes the air density ρ, the wing chord c and the slope an of the lift curve, which is expressed as

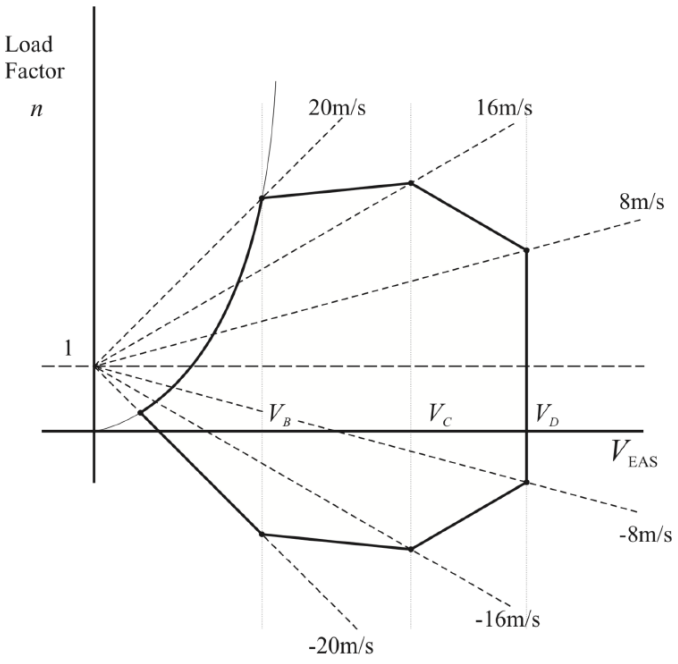

Figure 1. Gust envelop on a forward velocity vs aeroplane load factor (V-n) diagram.

Source: Wright and Cooper[2]

$$\mu_g \equiv \frac{2W}{Sa\rho cg} = \frac{2M}{Sa\rho c} \tag{3}$$

As the only variable in the revised definition of the gust mitigation factor K_g, it was introduced in the mid-1950s. This can be understood as the ratio between the peak normal acceleration of the discrete gust and the peak acceleration reference value of Equation 2 [3]. And this factor constitutes the famous modified gust load formula

$$\Delta n = \frac{1/2\,\rho aVU}{W/S} K_g \tag{4}$$

The introduction of K_g is necessary because lift build-up during gust penetration causes aerodynamic lag, and penetration of gust also causes a change in the angle of attack, which will cause the response of the aircraft. These effects are now incorporated into the functions Küssner (Ψ) and Wagner (Φ), respectively, because these effects are close to Küssner. where the sudden change in the angle of attack is explained by the Wagner function and the change in velocity is explained by the Küssner function. On the other hand, the variation of gust speed U and aircraft angle of attack with time can also be described as small step growth, therefore, the function Küssner (Ψ) and the function Wagner (Φ) can be expressed as exponential functions as

$$\Psi(t) = \frac{L_g(t)}{L_\alpha(\infty)} \quad and \quad \Phi(t) = \frac{L_\alpha(t)}{L_\alpha(\infty)} \tag{5}$$

In addition, the modified gust shape is also taken into account by the mitigation factor Kg. But real gusts can actually be represented by any shape, or by discrete gusts.

1.2.2, Discrete Gust Design Criteria (CS 25.341a)

Airworthiness authorities have required vertical and lateral gusts to be taken into account during the design phase of aircraft since the 1950s [1, 4]. The shape of the gust can be made as a typical '1 - cos' gust, which can be expressed mathematically as

$$U = \frac{U_{ds}}{2}\left(1 - cos\frac{\pi s}{H}\right) \quad for\ 0 \le s \le 2H \tag{6}$$

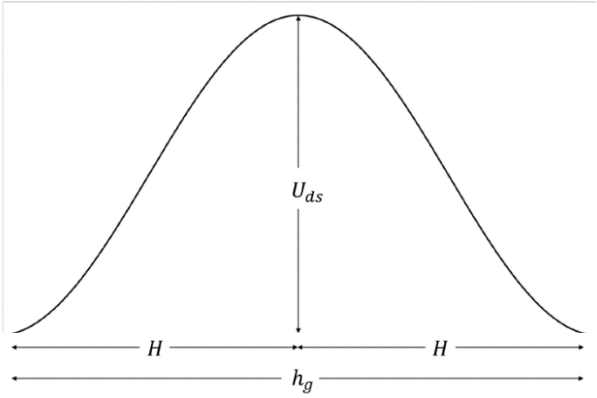

Figure 2. The typical shape of '1 - cos' gust, h_g is the total gust length, U_{ds} is the maximum design gust velocity and H is the gust gradient. Source: Simeone[5]

Assuming a constant relationship between a given point and time, the typical '1 - cos' shape As shown in figure 2. In equation (6), $\mathrm{U_{ds}}$ is the maximum design gust speed, s is the distance the aircraft penetrates into the gust, and H is the distance parallel to the flight path of the aircraft when the gust reaches its peak speed, or the gust gradient. $\mathrm{U_{ds}}$ can be expressed as

$$\mathrm{U_{ds}} = U_{ref} F_g \left(\frac{H}{107}\right)^{1/6} \tag{7}$$

where F_g is the flight profile mitigation factor and U_{ref} is the reference gust speed in the EAS, choose 107 as the denominator if using meters but 350 if using feet. The certification specification requires that all important structural degrees of freedom, including rigid body motion, and very aerodynamic properties are considered in the dynamic analysis. Then define the design limit load $\mathrm{P_{Li}}$ for a given load amount by equation (8)

$$\mathrm{P_{Li}} = P_{(\mathrm{lg})i} \pm P_{li} \tag{8}$$

where P_{li} is generated by considering the peak value of the time history of a series of individual "1 - cos" gust profiles, which represents the maximum incremental load defined by the peak value of the time history. $P_{(\mathrm{lg})i}$ is the 1g steady load of the amount of load under consideration indicated by the index i, which may be a load such as a bending moment.

On the other hand, what is sometimes called an all-weather gust analysis is sometimes considered necessary to deal with this situation, which results from the combined lateral and vertical action of wind gusts. It can be obtained by a linear combination of the load time histories due to pure vertical gusts and pure lateral gusts assuming combined gust loads.

1.2.3, Continuous Turbulence Design Criteria (CS 25.341b)

Section (b) of the CS-25.341 rule states that the ultimate loads that will act on the aircraft must be determined for all critical flight conditions of the aircraft such as altitude weight and weight and velocity profiles and the aircraft's dynamic response to continuous lateral and longitudinal turbulence. All important degrees of freedom and unsteady aerodynamic properties have been considered in the previous section, Discrete Gust Design Criteria. So now it is necessary to calculate the ultimate load due to continuous turbulence. It can be calculated by the following equation

$$\mathrm{P_{Li}} = P_{L(\mathrm{lg})i} \pm U_\sigma \bar{A}_i \tag{9}$$

where U is the ultimate turbulence intensity at true airspeed, the index i still represents the load type, and $\mathrm{P_{L(lg)i}}$ is the stable 1g load under this condition. $\mathrm{\bar{A}_i}$ is the ratio of the conditional rms incremental load to the rms turbulent velocity which can be determined by equation

$$\bar{A}_i = \sqrt{\int_0^\infty |H_i(\Omega)|^2 \Phi_{VK}(\Omega) d\Omega} \tag{10}$$

where $\mathrm{H_i}(\Omega)$ is obtained from the dynamic analysis and is a description of the relationship between the external atmospheric turbulence and the loads imposed on the structure, known as the frequency response function. $\Phi_{\mathrm{VK}}(\Omega)$ is the normalized power spectral density (PSD) of atmospheric turbulence as

$$\Phi_{VK}(\Omega) = \frac{\bar{L}}{\pi} \frac{1 + \frac{8}{3}(1.339\bar{L}\Omega)^2}{[1 + (1.339\bar{L}\Omega)^2]^{\frac{11}{6}}} \tag{11}$$

where L represents the characteristic scale wavelength of turbulence, which determines the normalized power spectral density (PSD) as a function of frequency, usually in feet, typically 2500 ft (762 in meter) to best t experimental data. V is the flight speed in m/s, and Ω is the calibration frequency in rad/m, which can be expressed as $\Omega = \omega/\mathrm{V}$. The constants of equation (11) are derived from von Kármán, a mathematical model of atmospheric turbulence that best matches experimentally observed data, known as the von Kármán spectrum.

1.3, Gast loads methodology

This section and the next two subsections will provide and describe the methods used today to meet the requirements set forth in the previous section.

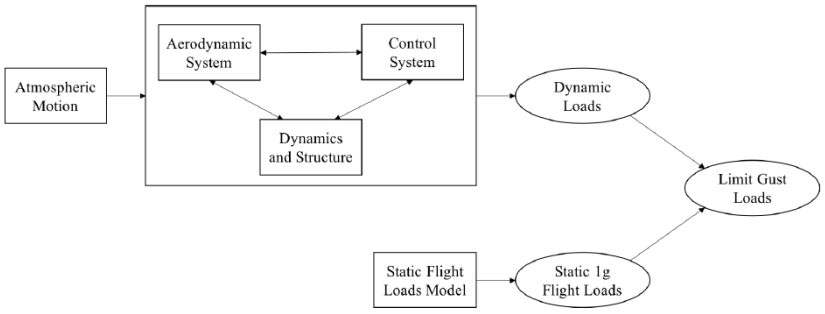

Figure 3. Basic system components for the analysis of gust response. Adapted from Certification Specification document (CS-25) [6].

In figure 3, the basic system components which are used to analyse the gust of the aircraft response are shown. The static aeroelastic method analyses a steady 1g flight load by defining basic external parameters such as speed, altitude, weight, and fuel load. Whereas a combination of a stable 1g flight load and a gust-inclusive incremental load can determine the ultimate or design gust load. When evaluating discrete gusts, the initial state of the aircraft should be assumed to be fine-tuned stable level flight. On the other hand, assessing continuous turbulence requires the assumption of average flight conditions for stable level flight of the construction. In order to achieve the maximum total load on each part of the aircraft, it is very important to ensure that such stable level flight conditions are selected, taking into account all possible effects such as from power settings and control surfaces.

Because of the interaction between the atmosphere, both the aircraft rigid and elastic motion and atmospheric turbulence are taken into account, which is the more complex nature of the process that leads to the calculation of gust incremental loads. Both linear analysis methods and nonlinear distraction methods may be part of this process. The application of linear analysis methods is justified when a linear model can effectively approximate the aircraft and its flight control system, such as simply superimposing incremental loads onto a steady level 1g load. However, the aircraft and its flight control system cannot necessarily be represented conservatively by the linear model, so it is necessary to introduce the nonlinear model. For example, when more pronounced nonlinear components of the excitation system and larger amplitudes of atmospheric turbulence appear, the linear model will no longer fit the aircraft and its flight control system. At this point some of the aircraft active control systems (e.g. torque performance and saturation, control law changes, rate and amplitude limiters, non-proportional feedback gains, etc.), autopilots, stabilization systems and load mitigation systems will become necessary to be considered the elements of. Nonlinear components usually need to be analysed in the time domain, because frequency domain methods are not suitable for modelling nonlinear components, and the complexity of the system is also increased by modelling nonlinear components.

In order to successfully model the aircraft when the linear analysis method calculates the ultimate loads, the following factors need to be considered. First, all rigid and flexible degrees of freedom of the aircraft must be described by the structural mechanics model, and enough flexible modes should be included in order to correctly reconstruct the aircraft's response to high-frequency excitations. In addition, mass and stiffness properties and damping properties are required in the model to complete the dynamics and structure part. The aerodynamics resulting from gust speed and aircraft response and steady-state and non-steady-state aerodynamic effects in the reduced frequency range will be described in the aerodynamic system section, including delays that should be applied in lift build-up when the aircraft enters the gust gradient. In addition, all interactions originating from the control components and operating modes associated with each component should be included and considered. Then, gyroscopic loads should also be taken into account in the gust analysis, which are caused by the engine and power assist passing through discrete gusts and continuous eddies. Finally, stability under discrete and continuous gust conditions is something that the dynamic model must be able to guarantee.

1.3.1, Discrete gust methods

A fairly simple method of meeting the certification requirements is described in the data item of the Engineering Science Data Unit (ESDU) technical series [3]. And this method is detailed in many books on loading and aeroelasticity [i.e. 2, 7].

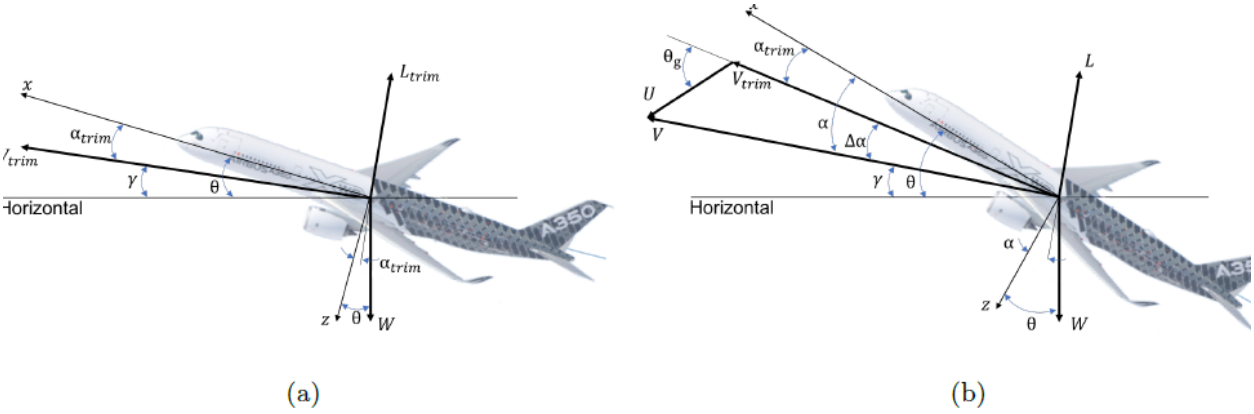

Figure 4. Comparing the motion coordinate system of the aircraft when encountering gusts (b) and when there is no disturbance in the atmosphere (a). Source: Simeone[5]

As shown in figure 4, the initial state of the aircraft is climbing flight conditions. This proposed defines the aircraft as a rigid aeroplane, and begins with its disposition response. The attack angle of the aircraft is α_{trim}, the pitch angle is θ. The V_{trim} is presented flight velocity and γ is the flight path angle. The L_{trim} is the lift of this rigid aeroplane, it is given by

$$L_{trim} = \frac{1}{2}\,\rho\,V_{trim}^2\,a\,S\,\alpha_{trim} \tag{12}$$

When the situation shown in figure 4 occurs, it means that it is input by a gust of wind. If the input gust is assumed to be a simple discrete '1 - cos' gust, the gust can be mathematically described as

$$U = \frac{U_0}{2}\left(1 - \cos\frac{\pi V}{H}t\right) \tag{13}$$

L represents the change in lift acting on the aircraft and can be written as

$$L = \frac{1}{2}\,\rho\,V^2\,a\,S\,\alpha = \frac{1}{2}\,\rho\,V^2\,a\,S\left(\alpha_{trim} + \Delta\alpha_g\right) \tag{14}$$

Where $\Delta\alpha_g \left(\approx \frac{U+\dot{z}}{V}\right)$ represents the increment of angle of attack due to the gust. during the gust encounter, the resulting velocity is presented by V. Equation 14 can be derived to the following differential equation with the Newton's second law's help.

$$M\,\ddot{z} = \frac{1}{2}\,\rho\,V^2\,a\,S\left(\alpha_{trim} + \frac{U + \dot{z}}{V}\right) \tag{15}$$

The acceleration increments defined in Equation 15 result from the acceleration response described above [3]. Then in order to extend the method to include the angle of incidence and the delay established by lift, the following differential equations of motion should be considered

$$M\,\ddot{z} + \frac{1}{2}\,V^2\,a\,S\int_0^t \Phi\{\mathrm{t}-\mathrm{t}^*\}\ddot{z}\{t^*\}dt^* = \frac{1}{2}\,V\,a\,S\int_0^t \Psi\{\mathrm{t}-\mathrm{t}^*\}\dot{U}\{t^*\}dt^* \qquad (16)$$

where $\Phi(\mathrm{t})$ is the Wagner function introduced earlier, and $\Psi(\mathrm{t})$ is the Küssner function introduced earlier. As shown in figure 5, the time t in $\Phi(\mathrm{t})$ and $\Psi(\mathrm{t})$ can be conveniently replaced by the dimensionless time τ, since they are only a function of the number of chord lengths passing through, and the dimensionless time τ is exactly equal to the progress of chord lengths. So the relationship between dimensionless time τ and time t can be expressed as

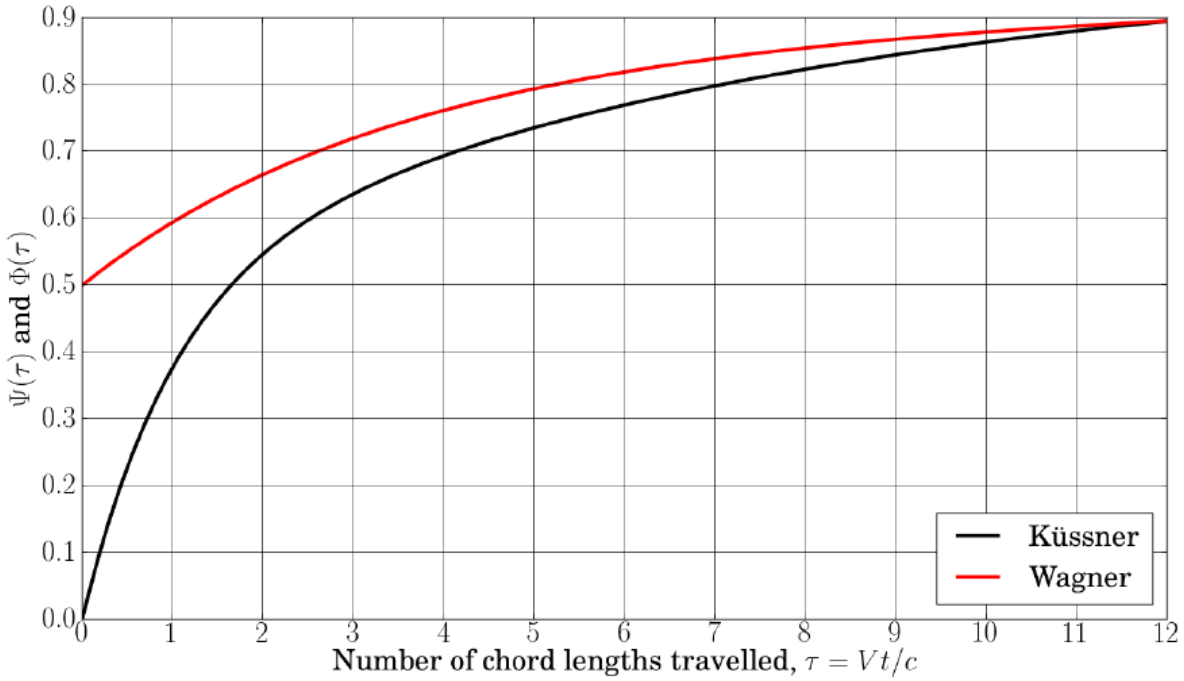

Figure 5. Wagner and Küssner function. Source: Simeone[5]

$$t = \frac{c\tau}{V}\,;\,\frac{d}{dt} = \frac{V}{c}\frac{d}{d\tau}\,;\,\frac{d^2}{dt^2} = \frac{V^2}{c^2}\frac{d^2}{d\tau^2} \qquad (17)$$

In addition, the Wagner function and the Küssner function can be defined as the following exponential functions to conveniently obtain their approximations

$$\Phi(\mathrm{t}) \approx 1.0 - 0.165\,e^{-0.0455\tau} - 0.5\,e^{-0.3\tau} \qquad (18)$$

$$\Psi(\mathrm{t}) \approx 1.0 - 0.5\,e^{-0.13\tau} - 0.5\,e^{-1.0\tau} \qquad (19)$$

Referring to figure 5, the images of the Wagner function and the Küssner function can explain how the gust build-up delay occurs when the aircraft enters the gust, they are 0.5 and 0 respectively when they are established, and then gradually approach equal over time. A sudden change in lift can be given by a sudden change in the angle of attack represented by Equation 18 and a sudden change in velocity represented by equation 19. So the dimensionless form of equation 16 can be written as

$$M\,\frac{V^2}{c^2}\frac{d^2z}{d\tau^2} + \frac{1}{2}\,V^2\,a\,S\int_0^\tau \Phi\{\tau-\tau^*\}\frac{V^2}{c^2}\frac{d^2z}{d\tau^2}\frac{c}{V}d\tau^* = \frac{1}{2}\,V\,a\,S\int_0^\tau \Psi\{\tau-\tau^*\}\frac{dU}{d\tau}\frac{c}{V}d\tau^* \qquad (20)$$

can then be rewritten as

$$\frac{d^2z}{d\tau^2} + \frac{1}{\mu_g}\int_0^{\tau} \Phi\{\tau - \tau^*\}\,\frac{d^2z}{d\tau^2}\,d\tau^* = \frac{1}{\mu_g}\,\frac{cU_{ds}}{V}\int_0^{\tau} \Psi\{\tau - \tau^*\}\,\frac{d}{d\tau}\left(\frac{U}{U_{ds}}\right)d\tau^* \tag{21}$$

Among them, $(\frac{U}{U_{ds}})$ can be obtained in the previous Equation 6, and the quality parameter μ_g is defined in the previous equation 3. The solution to equation 21 returns the non-dimensional time histories of $\frac{d^2z}{d\tau^2}$ and $\frac{dz}{d\tau}$, and gives numerically for a series of values of mass parameter μ_g. Then the incremental load factor can be obtained by considering the maximum value of $\frac{d^2z}{d\tau^2}$ as shown in the following equation

$$\Delta n = \frac{\ddot{z}}{g} = \frac{1}{g}\,\frac{V^2}{c^2}\,\frac{d^2z}{d\tau^2} = \frac{1}{g}\,\frac{V^2}{c^2}\,\frac{cU_{ds}}{V}\left(\frac{d^2z}{d\tau^2}\right)_{\frac{cU_{ds}}{V}=1} \tag{22}$$

Equation 23 can be turned into the following equation by multiplying and dividing by the μ_g

$$\Delta n = \mu_g \left(\frac{d^2z}{d\tau^2}\right)_{\frac{cU_{ds}}{V}=1} \frac{\rho U_{ds} V a}{2W/S} \tag{23}$$

The modified gust mitigation factor K_g can be defined and replaced by the first two terms on the right side of equation 23, μ_g and $\left(\frac{d^2z}{d\tau^2}\right)_{\frac{cU_{ds}}{V}=1}$, gust mitigation An approximation of the factor K_g can be empirically defined as

$$K_g = \frac{0.88\mu_g}{5.3 + \mu_g} \tag{24}$$

The pitch response of the aircraft into gusts can be considered by adding consideration to the additional degrees of freedom required for pitch motion to the currently employed rigid aircraft model. As shown in figure 4, these extra degrees of freedom make the relative centre of mass, and the positive nose up. The result of this is that an incremental lift ΔL_W acting on the aerodynamic center of the wing and an incremental lift ΔL_T acting on the aerodynamic center of the tailplane is generated.

$$\Delta L_W = \frac{1}{2}\,\rho\, V^2\, S_W\, a_W\,(\,\Delta\alpha_{gW}\,)\;\; and\;\; \Delta L_T = \frac{1}{2}\,\rho\, V^2\, S_T\, a_T\,(\,\Delta\alpha_{gT}\,) \tag{25}$$

where $\Delta\alpha_{gW}$ represents the increment of the wing angle of attack, and $\Delta\alpha_{gT}$ represents the increment of the angle of attack of the tailplane, which are defined as

$$\Delta\alpha_{gW} = \frac{U(t) + \dot{z}_W}{V} + \theta \;\; and \;\; \Delta\alpha_{gW} = \frac{U\left(t - \frac{l}{V}\right) + \dot{z}_T}{V} + \theta \tag{26}$$

where the heave velocity $\dot{z}_w$ of the aerodynamic centre of the wing is defined as $\dot{z}_w = \dot{z} - l_W\,\dot{\theta}$, and the heave velocity $\dot{z}_T$ of the aerodynamic centre of the tailplane is defined as $\dot{z}_T = \dot{z} - l_T\,\dot{\theta}$. The distances from the center of mass of the aircraft to the aerodynamic centers of the wings and tail are written as l_W and l_T, respectively. l/V is the amount of time given by the distance between the wing and tail aerodynamic centre divided by the speed of the aircraft. Incremental heave and pitch responses can be

obtained from the solution to the equations of motion of the aircraft obtained by combining Equation 25 and equation 26 with Newton's second law. Can be written in compact form

$$\begin{bmatrix} M & 0 \\ 0 & I_y \end{bmatrix} \begin{Bmatrix} \ddot{z} \\ \ddot{\theta} \end{Bmatrix} + \begin{bmatrix} -Z_{\dot{z}} & -Z_q \\ -M_{\dot{z}} & -M_q \end{bmatrix} \begin{Bmatrix} \dot{z} \\ \dot{\theta} \end{Bmatrix} + \begin{bmatrix} 0 & -Z_{\dot{z}} \\ 0 & -M_{\_\dot{z}} \end{bmatrix} \begin{Bmatrix} z_C \\ \theta \end{Bmatrix} = \begin{Bmatrix} -Z_{gW} \\ -M_{gW} \end{Bmatrix} U(t) + \begin{Bmatrix} -Z_{gT} \\ -M_{gT} \end{Bmatrix} U\left(t - \frac{l}{V}\right) \quad (27)$$

where pitch moment of inertia is written l_y and gust related derivatives (shown in Appendix 1), rate of heave $\dot{z}$, rate of change of pitch $\dot{\theta}$ and longitudinal aerodynamic derivatives for the change of pitch θ are introduced to simplify the equation. In this case the aircraft's response becomes more refined by adding the tail's influence to the wing. In the case of a '1 - cos' gust, the aircraft initially has a negative heave acceleration that pushes it up and pitches up due to the increased lift on the seats of the wings, while the gust reaching the tail will cause the lift The heave acceleration becomes positive and pitches the nose of the aircraft down. This keeps the aircraft away from the forced motion caused by gusts, as the heave acceleration pushes the aircraft down and puts it in a free-response state.

The generalized form of the equation of motion for time-domain gust analysis is shown below

$$\bar{M}\,\ddot{q} + (\,\rho\,V\,\bar{C} + D\,)\,\dot{q} + \rho\,V^2\,\bar{E}\,q\ *\Phi + \ \bar{K}\,q\ = \rho\,V\,R_{gW}\,U(t) * \Psi\ + \rho\,V\,R_{gW}\,U\ \left(1 - \frac{l}{V}\right) *\ \Psi \quad (28)$$

where * represents the convolution integral of Wagner and Küssner, and the gust-related aerodynamic vectors R_{gW} and R_{gT} of the wing and tail are shown below

$$R_{gW} = \begin{Bmatrix} Z_{gW} \\ M_{gW} \end{Bmatrix} \ and \ R_{gT} = \begin{Bmatrix} Z_{gT} \\ M_{gT} \end{Bmatrix} \quad (29)$$

On the other hand, unsteady aerodynamic effects need to be considered in Wagner and Küssner

1.3.2, Continuous turbulence methods

The Fourier transform of the system's impulse response function H_{Im}, or the system's transfer function (or FRF), and the power spectral density (PSD) through random variables are commonly used to deal with continuous turbulent responses. The FRF of the system can be expressed as

$$H(i\omega) = \int_0^\infty H_{Im}\,(t)\,e^{-i\omega t}\,dt \quad (30)$$

where rad/s will be used as the unit of ω. It should be noted that the implicit property of how the system behaves under harmonic excitation of any frequency is the description object of the transfer function, and if expressed in terms of the relationship between output and input, it can be written as

$$\Phi_O(\omega) = \ |H(i\omega)|^2\ \Phi_I(\omega) \quad (31)$$

The power spectral density function of the random input perturbation of the linear system in equation 31 is denoted by $\Phi_I(\omega)$, and the power spectral density function of the output of the linear system is denoted by $\Phi_O(\omega)$. In this aspect of gust analysis the power spectral density of a random input perturbation of a linear system is representative of the gust input, while a given amount of load for a rigid or flexible aircraft such as how the bending moment at a given wing station relates to the input gust velocity All frequencies of interest can be used to determine the transfer function of the aircraft, and the output power spectral density function is provided by Equation 11. As stated in the Discrete Gust Design

Criteria (CS 25.341a) above, the shape of the von Kármán spectrum, as shown in figure 6, is the shape of the input gust that is primarily required by the authorities.

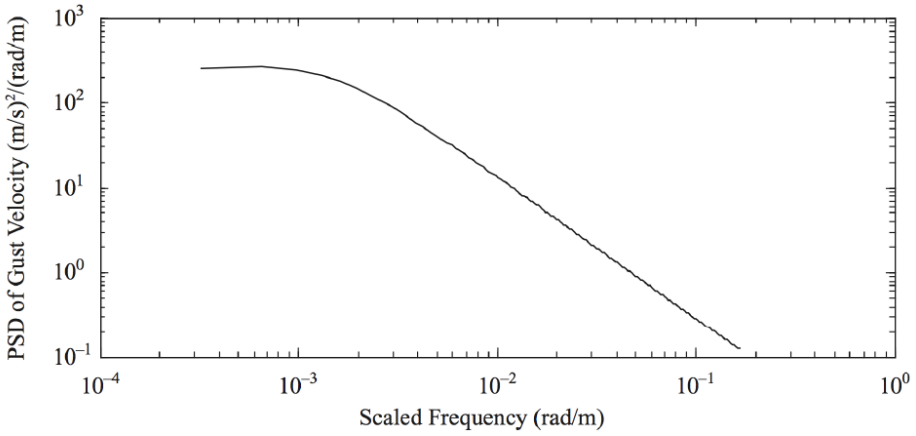

Figure 6. von Kármán spectrum power spectral density function. Source: Simeone[5]

As shown in figure 6, the higher and lower frequencies of the von Kármán spectrum are separated by its characteristic 'knee'. The scale of the turbulence $\bar{L}$ determines the location of this 'knee', and the frequency at which the 'knee' occurs increases as the scale of turbulence decreases, which in turn leads to a constant frequency range increase in power spectral density. The scale-dependent definition and meaning of turbulence is still debated, so it does not currently have a correct value, but since values above 2500 feet do not have an effect on higher frequencies where gust affects the aircraft response, it is appropriate for design use value. To sum up, equation 9 , equation 10 and equation 11 can determine gust limit loads

1.4, Aerodynamic and aeroelastic models

To complete the gust reconstruction, increasingly complex different aerodynamic and aeroelastic models are proposed, since the gust load reconstruction should be covered in different design stages. This work is mainly based on the airfoil of the 2 degree of freedom (Dof) nonlinear model with Theodorsen's aerodynamics as the analytical model.

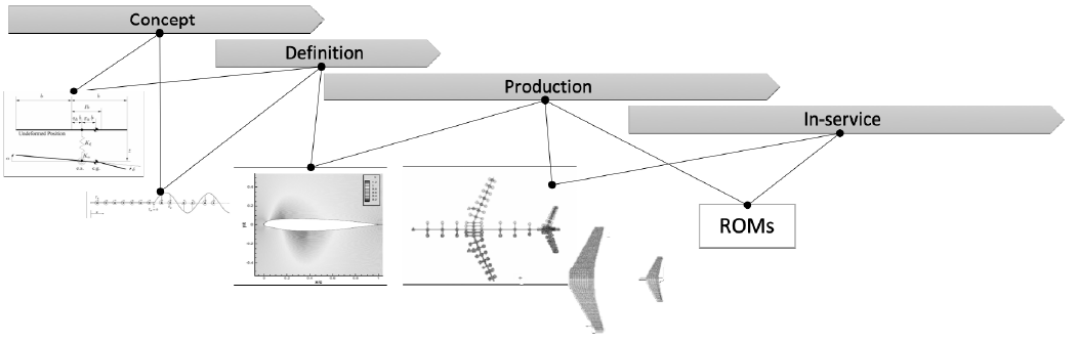

Figure 7. Models that should be used in different design stages. From right to left: ROMs, 3D beam-stick with DLM, CFD model, ULVM model, 2DoF model

Figure 7 shows the aerodynamic and aeroelastic models used in the different design stages of the aircraft. In order from left to right, first, the 2Dof model of the wing is considered immersed in an incompressible 2D flow, which is based on Theodorsen's aerodynamics, modeling of structural nonlinearities and trailing edge flaps Feasible. The second model is a plate in a potential flow that only considers aerodynamic effects. Similar to the first approach, it is applied to the design of the aircraft at the concept stage, where the expensive design is out of scope because a concise and detailed model of the aircraft has not been created. Unsteady lumped vortex method (ULVM) modeling was applied to the flat plate and its flow unsteadiness was verified according to Theodorsen theory. When entering a "gusty" environment, delay in the building up of the lift can be verified by Küssner and Wagner. Often, such a model can serve as an early indicator of the compatibility of the model and a demonstration of the applicability of reconstruction methods used in the conceptual phase of an aircraft design, and thus can be considered a prototype for higher fidelity CFD simulation. Detailed aerodynamic and aeroelastic analysis is used in the later stages of aircraft design when performed under different conditions using higher complexity models. This also makes CFD simulation computationally expensive and cannot be used in service. To ensure the safe operation of the aircraft, the preservation of high-precision results is a must for these analyses. Therefore, in order to extract the critical gust loads to reduce the size of the aircraft, rapid modeling of the response of the aircraft to turbulence and gusts is required, optionally applying intermediate reduced order models (ROMs).

The 2 degree of freedom (Dof) nonlinear model with Theodorsen's aerodynamics method used in this work will be introduced in detail in the methodology section.

1.5, Inverse methods

The inverse method means that the standard method of reconstructing the unknown input force is based on a method in the frequency domain that assumes a linear and invertible system. Because the Fourier transform and the inverse transform are involved in the inverse method, the Fourier transform, and the inverse transform are only valid in the linear state, which leads to the inverse method requiring the system to be linear. But several related studies have attempted to apply inverse methods to nonlinear systems, such as extended Kalman filters and recursive least squares estimators or iterating the inverse methods. But extended Kalman filters and recursive least squares estimators work in the time domain, while the inverse method iterates over multiple iterations and further user interaction to complete the overall convergence.

Deconvolution is the most commonly used technique for inverse analysis of excitation force reconstruction. Assuming that the excitation force is linearly dependent on the system response and the deformation of the object is negligible, it can be expressed by the linear convolution integral equation 1.

$$a(t) = h(t) * f(t) \tag{32}$$

Where a(t) is the measured response of the object at one point, f(t) is the excitation force, h(t) is the impulse response function of the system, and * denotes the convolution operation. When entering the frequency domain, convolutions can be transformed into simple algebraic multiplications via Fourier transforms. It is possible to Fourier transform the input f(t) to F(ω), a(t) to A(ω) and h(t) to H(ω), where ω represents frequency. H(ω) represents the frequency response function (FRF) of the system, which describes the performance of the system under different frequencies of harmonic excitation and is an implicit property. The relationship between input and output can be expressed as

$$H(\omega) = \frac{A(\omega)}{F(\omega)} \tag{33}$$

Fast Fourier Transforms (FFTs) are computationally simpler than solving convolution integrals in the time domain. However, since the Fourier transform is prepared for infinitely continuous signals, it is necessary to solve the problem by truncation when dealing with the FFT algorithm. Also, truncation can introduce errors due to the resulting discontinuities at the extreme values of the finite dataset. So the magnitude of these errors needs to be reduced by applying windowing functions to the data.

Although in the case of using industrial models, the inverse method can give a good result. However, there is a lack of consistency in the results obtained using nonlinear models [5]. The structure of modern aircraft is gradually complicated, and the control system is also nonlinear, so for modern situations, it is necessary to consider a nonlinear reconstruction scheme.

1.6, Optimisation methods

Optimisation methods are time-domain methods, and they are used in contrast to frequency-domain methods when explicit simulation of nonlinearity is required. This is because, in nonlinear problems, the effects of different loads can be very different, making the problem difficult to linearise. Two main branches, gradient-free optimisation methods and gradient-based optimisation methods, will be introduced here.

The gradient-free optimisation method means that it is ideal for solving non-smooth or discontinuous functions and does not rely on gradient information. But since each iteration requires a direct evaluation of the function, it takes longer to solve the problem using them. So they are more suitable for solving computationally difficult problems. Most of the time, they are developed as global optimisers because of their ability to find a global optimum and multiple local optima. Common algorithms include genetic algorithm, simulated annealing, segmentation rectangle method, particle swarm optimisation and Nelder-Mead simplex method (non-linear simplex method).

Gradient-based optimisation methods should be used as the direction to search for the minimum value of a function because they can solve problems with a large design space and a large number of design variables. The fast convergence speed of this type of optimisation method results in very high computational efficiency, and it also provides explicit convergence criteria. But when there are multiple local minima, such optimisation methods may fail to provide a global minimum. So it should be overcome by searching the design space from random different starting points. They are mainly based on four steps to complete. The first is the convergence test; when the convergence condition is satisfied, the search will stop. Then calculate the search direction, and then calculate the step size. Finally, the design variables are updated, the new variables obtained are stored, and the number of iterations is updated before starting the convergence test.

For a realistic situation, since the input data is all extracted from the flight data recorder, measurement noise from the aircraft instruments is also recorded in the data, potentially interfering with the gust reconstruction. This results in the need to pre-process the data by passing it through appropriate digital filters. On the other hand, the low sampling rate of the flight data recorder needs to be considered. Since this can result in very discrete data points, interpolation techniques and proper filtering need to be considered to ensure the correct functioning of the reconstruction framework.

The results of the reconstruction are subject to errors and uncertainties. To obtain an accurate gust profile reconstruction requires the most complex aircraft model to capture the full interaction between the gust and the aircraft structure. But increased structural complexity is often accompanied by more expensive simulations, so the right balance needs to be struck. In addition, the wrong reconstruction can also be caused by wrong input data.

1.7, Machine learning

Nowadays, the application of machine learning is more and more extensive, and there are more and more applications in the related fields of aircraft design. Since the gust load studied in this research project is related to the damage of the aircraft structure and the material failure in the aircraft structure, The literature has been read in this direction.

In the literature, methods to identify damage in aircraft structures using self-powered sensing techniques have been proposed through machine learning techniques [8,9]. Because the data fed back by sensors in the system is nonlinear, and the feedback of information has the problem of delay synchronization. To solve this problem, it is necessary to analyse the discrete and time-delayed binary data to extract enough reliable information to complete the interpretation and prediction of the data. So a method combining low-rank matrix completion, PR, k-nearest neighbour and data fusion model is proposed to solve the above problem [2]. On the other hand, in the related research on localization acting on aircraft surface impact events, a localization method using acoustic emission (AE) as a monitoring method, random forest and deep learning to train the source location model was proposed [10]. This method is to reduce the number of sensors carried as much as possible while obtaining accurate impact position results.

The following will introduce the theory of these two applied machine learning methods, as well as the theory and working of Regression trees, a branching algorithm of the Decision tree algorithm that will be mentioned in the discussion part.

1.7.1, Deep learning

When neural networks were invented decades ago, the original motivation was to write programs that could mimic the learning and thinking of biological brains. Even now that neural networks, or artificial neural networks, are very different from what anyone thinks the brain does to work and learn, some biological motivations remain in neural networks.

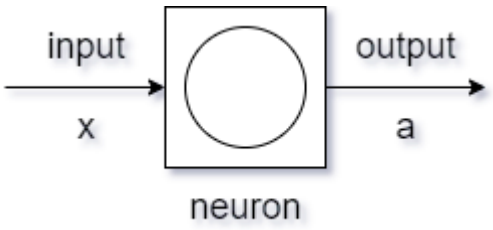

Figure 8. Mathematical model in artificial neural network

As shown in figure 8, the artificial neural network uses a very simple mathematical model to accomplish what the Biological neuron does. Input a feature, this feature is a number, perform some operations in the neuron, and finally output a feature, the output feature is also a number, this output number may be called the output feature of the next neuron. Therefore, it can also be considered that a neuron represents

a microcomputer whose only job is to input one or a few numbers and output a number. Usually when building an artificial neural network, it is necessary to simulate many neurons at the same time, as shown in figure 8 In this case, the combination of multiple neurons is called a layer. The layer that outputs the last feature is called the output layer, and the other layers before it are called the hidden layer. Except for the first layer, the input features of the next layer are the input features of the previous layer

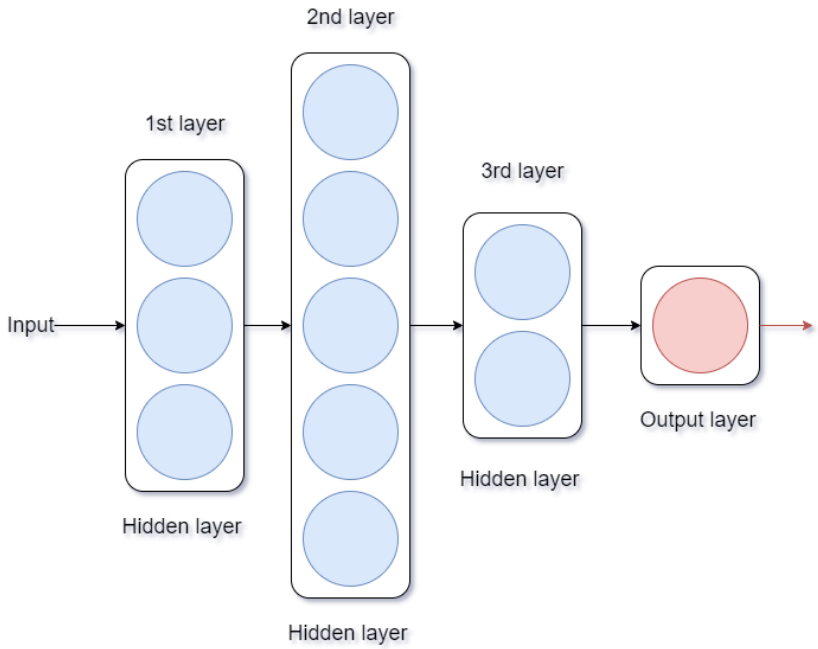

Figure 9. Multiple Hidden layers artificial neural network

1.7.2, Decision tree

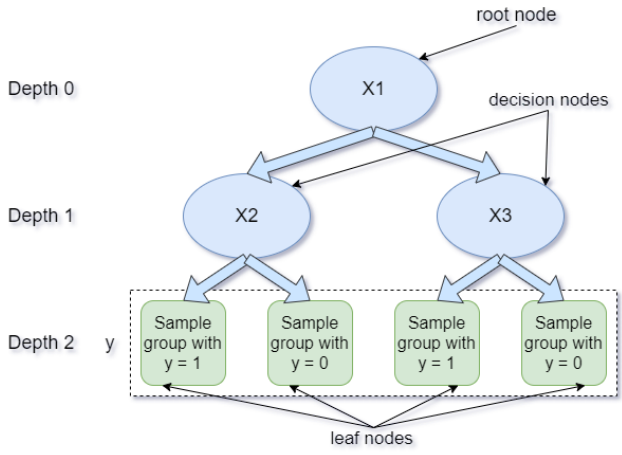

	X1	X1	X1	y
sample 1	1	1	0	1
sample 2	1	0	0	0
sample 3	0	0	0	0
sample 4	1	1	1	1
sample 5	0	1	0	1
sample 6	1	0	1	1

Figure 10. Decision tree

As shown in figure 10, the decision tree consists of multiple nodes. The circles represent decision nodes. These nodes represent the features of the input samples, represented by x, and classify these features at this node. The boxes represent leaf nodes, which represent the output results, represented by y. The

decision nodes at the top are called root nodes, where the first classification of the input samples is performed. Depth represents the distance from the node to the topmost root node.

The purpose of the decision tree is to classify the different features of the input samples, and finally filter out the corresponding samples with the same output y. The learning process of the decision tree first determines the features classified by the root node. Classify the learning examples by the root node and enter the decision node of the next depth. After Examples enter the next depth, summarize the features that can be distinguished in each group, and select the most effective features to classify again. Repeat the above learning process until the output leaf nodes are reached, and stop splitting.

When judging whether to stop splitting, you can judge in the following ways. First, when the purity of the y value corresponding to the sample assigned by the node is equal to 100%, splitting can be stopped. The second case is to stop splitting when splitting a node causes the depth of the tree to exceed the maximum depth. This means that all features that can be used to distinguish samples have been used and cannot be split. In the third case, when the purity of the y value corresponding to the sample allocated by the node is higher than the set threshold, splitting can be stopped. Finally, when the number of samples allocated in the node is lower than the set threshold, the splitting is stopped.

As to which feature should be used to distinguish decision nodes, we can find the feature with the highest purity of the y value corresponding to the two groups of samples after classification.

Measuring Purity

Divide the sample by calculating the purity of the sample.

$$p = \frac{n}{n_{total}} \tag{34}$$

As shown in equation 34, n is the number of samples with a y value equal to 1 and n_{total} is the total number of samples. The p1 represents the percentage of samples with a y value equal to 1 in this group of samples, and the entropy $H(p_1)$ of this group of data is calculated by p. The calculation formula is shown below.

$$H(p_1) = -p_1 log_2(p_1) - p_0 log_2(p_0) \tag{35}$$

In equation 35, p_0 represents the percentage of samples with y equal to 0 in this group of samples. Here it can be calculated by $p_0 = 1-p_1$. So equation 36 can be derived.

$$H(p_1) = -p_1 log_2(p_1) - (1 - p_1) log_2(1 - p_1) \tag{36}$$

It should be pointed out here that in equation 36 if there is a situation of $0\log_2(0)$, it should be regarded as $0\log_2(0) = 0$.

Choosing a split

Because the total amount of samples in each group is different after being classified, it should be calculated by weighting when considering the selection of splits.

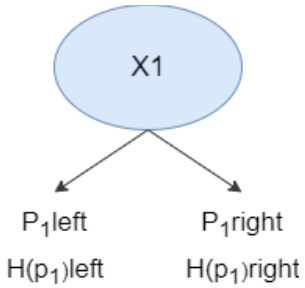

Figure 11. Decision node

As shown in the figure 11, after a decision node is split, the p_1 assigned to the left sample group is written as p_1^{left}, and p_1^{right} is the p_1 assigned to the sample group. Through these, the entropy of these two sets of samples is calculated, denoted as $H(p_1^{left})$and $H(p_1^{right})$.

$$Information\ Gain = H(p_1^{root}) - \left(w^{left}(p_1^{left}) + w^{right}(p_1^{right})\right) \quad (37)$$

As shown in equation 37, $H(p_1^{root})$ represents the total p_1 of the sample group input to this split. w^{left} and w^{right} represent the percentage of the total sample size assigned to the left and the percentage of the total sample size assigned to the right, respectively. The purity of different groups can be compared by the size of the information gain.

One-hot encoding

When there are multiple types of a feature of a sample, in order to facilitate learning, the feature can be split by the One-hot encoding method, as shown in the following figure.

	X1			a	b	c
sample 1	a		sample 1	1	0	0
sample 2	b		sample 2	0	1	0
sample 3	a		sample 3	1	0	0
sample 4	a		sample 4	1	0	0
sample 5	c	One-hot encoding	sample 5	0	0	1
sample 6	c		sample 6	0	0	1
sample 7	b		sample 7	0	1	0
sample 8	c		sample 8	0	0	1
sample 9	a		sample 9	1	0	0
sample 10	c		sample 10	0	0	1

Figure 12. One-hot encoding

After splitting, the types of all features are represented by 1 and 0. When the sample has this feature, the sample is divided into 1, and when it does not have this feature, the sample is divided into 0.

Continuous Valued features

Different from many decision tree application scenarios, all features in this project exist as continuous data. For these data, the above methods cannot extract features efficiently, so the split choosing method for Continuous Valued features should be introduced.

Calculate the information gain of these points separately by trying to choose different x in them. By comparing these information gains, the most suitable point for splitting is selected as the splitting criterion for decision nodes.

Regression trees

In this project, the y that needs to be classified is not 0 or 1 but a series of values. Therefore, regression trees, which output numerical values, should be used.

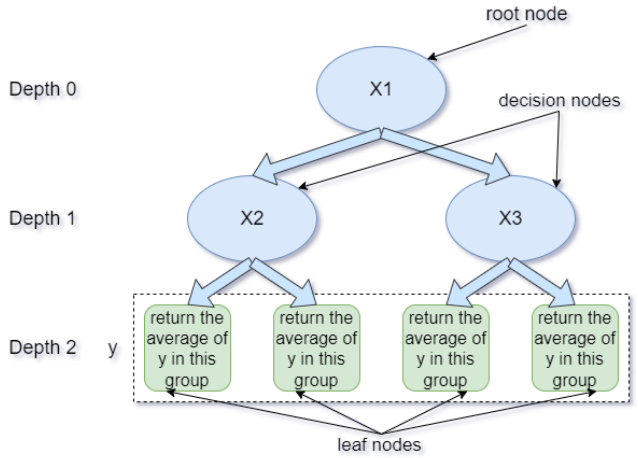

	X1	X1	X1	y
sample 1	1	1	0	n1
sample 2	1	0	0	n2
sample 3	0	0	0	n3
sample 4	1	1	1	n2
sample 5	0	1	0	n4
sample 6	1	0	1	n4

Figure 13. Regression trees

As shown in the figure 13 above, regression trees are methods by classifying samples and predicting the value of y. In this method, the method of selecting split is shown in the following equations.

$$information\ gain = v_r - \left(w^l \cdot v_1 + w^r \cdot v_2\right) \tag{38}$$

$$w^l = \frac{n_l}{n_{root}} \tag{39}$$

$$w^r = \frac{n_r}{n_{root}} \tag{40}$$

where v_1 and v_2 represent the variance of the y-values assigned to the left and right samples, respectively, and v_r represents the variance at the root. Then, w^l and w^r represent the percentages of the left and right samples to the total number of samples, respectively, which can be calculated by equation (39) and equation (40).

Sampling with replacement

Sampling with replacement is a key module for building tree collections. To complete Sampling with replacement, it is necessary to establish multiple random training sets, randomly extract data from the total data set and save them in a set. Some data has not been extracted.

random forest

The random forest algorithm is a better algorithm than using a single decision tree. To complete this algorithm, the first step is to generate a tree sample. This tree sample needs to use the Sampling with replacement method, and then generate a decision through this tree sample. tree. Repeat the above steps, you will get a slightly different decision tree, repeat these steps many times, usually the recommended value repeats between 64 and 228, because after the number of repetitions exceeds a certain value, the income will be increased due to the increase in calculation cost. gradually decreases. When done, when a prediction needs to be made, let those trees all vote for the correct final prediction

On the other hand, because of the replacement of data, the decision tree will explore very small changes, and because the random forest trains multiple decision trees, it is equivalent to averaging these small changes. So small changes in the input data are unlikely to have a huge impact on the overall output.

2, RESEARCH AIMS AND OBJECTIVES

2.1, main purpose

Although in the case of using industrial models, the inverse method can give a good result. However, there is a lack of consistency in the results obtained using nonlinear models. The structure of modern aircraft is gradually becoming more complex, and the control system is also nonlinear, so for modern situations, nonlinear reconstruction schemes need to be considered. However, for the optimization method suitable for nonlinear problems, the reconstruction results are affected by errors and uncertainties. If you want to obtain an accurate reconstruction of the gust profile, the most complex aircraft model is required to capture the relationship between the gust and the aircraft structure. all interactions between them. But increased structural complexity is often accompanied by more expensive simulations, so the right balance needs to be struck. In addition, wrong reconstructions can also be caused by wrong input data. Therefore, the idea of gust reconstruction based on machine learning method is proposed, and the main goal of this project is to propose and verify the feasibility of applying the algorithm in machine learning method to gust reconstruction.

2.2, main target

To achieve the main purpose of this study, the following objectives have been addressed

Creating a Machine Learning Algorithm for Gust Reconstruction

The Aerodynamic and aeroelastic models of the aircraft selected for this study are the 2 degree of freedom nonlinear model with Theodorsen's aerodynamics. From the equations of motion of this type of model, a linear regression model is created.

Testing of Machine Learning Algorithms

After a lot of attempts on the linear regression model, the regression of the gust data slice was finally completed and the problems of the proposed method were found.

3, METHODOLOGY

3.1, 2DoF nonlinear model

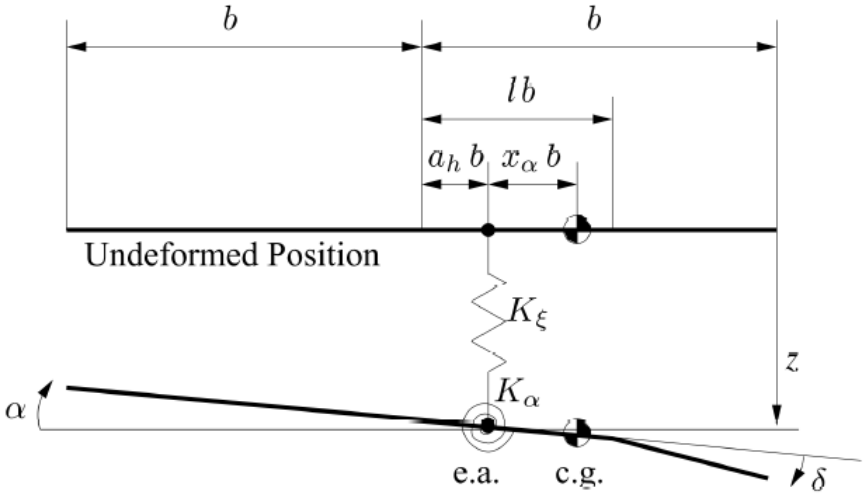

Figure 14. 2Dof Aerofoil section with trailing edge flap.

Figure 14 shows a 2 degrees of freedom (Dof) Aerofoil moving around a reference elastic axis (e.a.). The angle of attack α which about the elastic axis is positive upward, and the positive downward plunge deflection is denoted by z. A massless trailing edge flap with hinge is provided at the rear of the air foil, and lb represents its distance from the central axis of the wing. The flap deflection is denoted by δ, the reference frame used for the angular magnitude of δ is not defined relative to the wind direction, but is defined relative to the position of the trailing edge flap when it is not deflected. two springs K_α and K_ξ, restrain the motion of aerofoil, and assumed when $z = \alpha = \delta = 0$ the motion of aerofoil have a horizontal equilibrium. The system also contains modelling an incompressible two-dimensional flow as in Theodorsen [11, 12] gives the aerodynamics and the structural damping that occurs in each degrees of freedom. To study the structural effects of nonlinearity, nonlinear terms are added to the equations of motion. In dimensional form, the Lagrange formulation [13] is pushed to the following equation by adding non-linear restoring forces to pitch and dive

$$m\ddot{z} + S_\alpha\ddot{\alpha} + C_\xi\dot{z} + K_\xi\left(z + \beta_\xi z^3 + \beta_{\xi_5} z^5\right) = -L \tag{40}$$

$$S_\alpha\ddot{z} + I_\alpha\ddot{\alpha} + C_\alpha\dot{z} + K_\alpha\left(\alpha + \beta_\alpha z^3 + \beta_{\alpha_5} z^5\right) = M \tag{41}$$

The polynomial brought by the Taylor series expansion can approximate the structural nonlinearity. According to the usual notational conventions in aerodynamics, the dive displacement z is defined as a positive downward direction and the lift L is defined as a positive upward direction. In other cases, M represents the total mass of the aircraft, where M represents the pitch moment. The equations of motion can be transformed into nondimensional form as

$$\xi'' + x_\alpha \alpha'' + 2\zeta_\xi \frac{\overline{\omega}}{V^*}\xi' + \left(\frac{\overline{\omega}}{V^*}\right)^2 \left(\xi + \beta_\xi \xi^3 + \beta_{\xi_5}\xi^5\right) = -\frac{1}{\pi\mu} C_L\left(\tau_{\frac{1}{2}}\right) \quad (42)$$

$$\frac{x_\alpha}{r_a^2}\xi'' + \alpha'' + 2\zeta_\alpha \frac{1}{V^*}\alpha' + \left(\frac{1}{V^*}\right)^2 \left(\alpha + \beta_\alpha \alpha^3 + \beta_{\alpha_5}\alpha^5\right) = -\frac{1}{\pi\mu r_a^2} C_m\left(\tau_{\frac{1}{2}}\right) \quad (43)$$

Dimensionless parameters are defined in Nomenclature. Here the non-dimensional parameters $\tau_{\frac{1}{2}}$ and $\dot{()} = V/b()'$ are used in place of the differentiation with respect to t represented by $\dot{()}$. $C_L\left(\tau_{\frac{1}{2}}\right)$ and $C_m\left(\tau_{\frac{1}{2}}\right)$ consist of three parts and represent the total aerodynamic load. These three components are shown in the formula below

$$C_L\left(\tau_{\frac{1}{2}}\right) = C_L^{foil}\left(\tau_{\frac{1}{2}}\right) + C_L^{\delta}\left(\tau_{\frac{1}{2}}\right) + C_L^{gust}\left(\tau_{\frac{1}{2}}\right) \quad (44)$$

$$C_m\left(\tau_{\frac{1}{2}}\right) = C_m^{foil}\left(\tau_{\frac{1}{2}}\right) + C_m^{\delta}\left(\tau_{\frac{1}{2}}\right) + C_m^{gust}\left(\tau_{\frac{1}{2}}\right) \quad (45)$$

Among them, $C_L^{gust}\left(\tau_{\frac{1}{2}}\right)$ and $C_m^{gust}\left(\tau_{\frac{1}{2}}\right)$ represent the total load caused by the penetration gust, $C_L^{\delta}\left(\tau_{\frac{1}{2}}\right)$ and $C_m^{\delta}\left(\tau_{\frac{1}{2}}\right)$ represents the total load caused by flap deflection, $C_L^{foil}\left(\tau_{\frac{1}{2}}\right)$ and $C_m^{foil}\left(\tau_{\frac{1}{2}}\right)$ represent the airfoil movement total load. Generalize the convolution integral to time histories considering the Wagner and Küssner functions in terms of exponential approximations introduced in equation 19 and equation 18. Equation 42 and Equation 43 are difficult to solve because they are integro-differential equations (IDEs) that need to be converted into ordinary differential equations (ODEs) [12]. Then in state space form, the equations of motion can be written as

$$\frac{dw}{d\tau_{\frac{1}{2}}} = R\left(w, u_c, u_d\right) \quad (46)$$

Among them, the n-dimensional state-space vector is represented by w, w includes the aerodynamic state and α, α', ξ, ξ', and the nonlinear residual is represented by R. The flap deflection related δ, δ' and δ'' are included in the input vector u_c. Whereas any external disturbance acting on the system is described by a vector u_d.

3.2, Linear regression method

Complete the reconstruction of the gust model by establishing the linear regression model of the gust shape

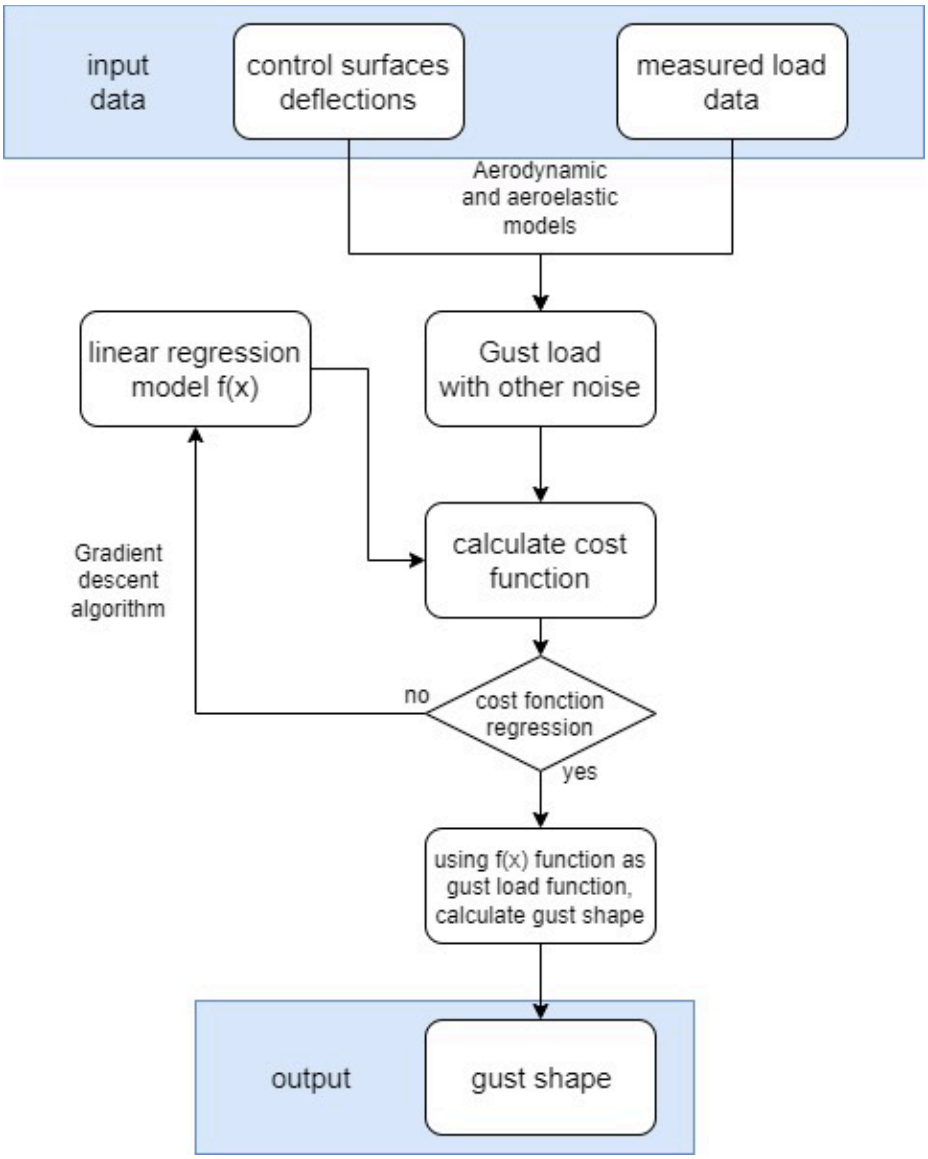

Figure 15. Flowchart for reconstruction of gust using linear regression method

As shown in the flow chart, the process of regression algorithm through machine learning requires four steps. The time history and measured load data of control surface deflections (acceleration, rates, Euler angle, etc.) are the data the algorithm needs to prepare for running. The gust load, including other noise, is calculated by known aerodynamic and aeroelastic models. First, establish a linear regression model f(x), f(x) can be expressed as

$$f(x) = \vec{w} \cdot \vec{a} + b \tag{47}$$

Among them, b is a constant and $\vec{x}$ and $\vec{w}$ are vectors, where $\vec{x}$ is a variable containing m features, and $\vec{w}$ includes the constant terms corresponding to all elements in $\vec{x}$.

n the second step, by comparing the output of f(x) with the gust load containing other noises, cost $J(\vec{w}, b)$ is obtained by calculation, cost $J(\vec{w}, b)$ can be shown as

$$J(\vec{w},b)=\frac{1}{2m}\sum_{i=1}^{m}(f(x)_i-y_i)^2 \tag{48}$$

where y represents the gust load with other noise. Then change the $\vec{w}$ and b of the linear regression model through the gradient descent algorithm, and calculate the cost $J(\vec{w},b)$ again using the model with updated w and b. After many iterations, the cost function is obtained, and whether the regression model is close to the gust load function is confirmed by judging whether the cost function converges. If the function converges, use f(x) to calculate and output the gust shape. The gradient descent algorithm is expressed as

$$w_n=w_n-\alpha\frac{1}{m}\sum_{i=1}^{m}(f(x)_i-y_i)x_i \tag{49}$$

$$b=b-\alpha\frac{1}{m}\sum_{i=1}^{m}(f(x)_i-y_i) \tag{50}$$

where α is the learning rate, which determines the learning step size. Since the gust function contains multiple features, to avoid overfitting, the function should be adjusted through regularization and tried various times to obtain the most suitable regression model. When using regularization, the cost $J(\vec{w},b)$ and gradient descent algorithm can be expressed as

$$J(\vec{w},b)=\frac{1}{2m}[\sum_{i=1}^{m}(f(x)_i-y_i)^2+\frac{\lambda}{2m}\sum_{j=1}^{n}w_j^2] \tag{51}$$

$$w_n=w_n-\alpha\frac{1}{m}[\sum_{i=1}^{m}(f(x)_i-y_i)x_i+\frac{\lambda}{m}w_n] \tag{52}$$

$$b=b-\alpha\frac{1}{m}\sum_{i=1}^{m}(f(x)_i-y_i) \tag{53}$$

As mentioned above, $\frac{\lambda}{2m}\sum_j^n w_j^2$ can control w_j to a small value, so the regularization term can be used to adjust the function to avoid overfitting.

There are several points to note in the experiment. First, the choice of learning rate α will have an impact on the results. When the learning rate is too large, the minimum value to be learned may be crossed because the step size is too long, resulting in non-convergence of the final learning result. In addition, the selection of the initial $\vec{w}\ and\ b$ also has a great impact on the learning results. Choosing an inappropriate $\vec{w}\ and\ b$ may cause the cost to find the local minimum instead of the global minimum.

4, Resalt

The results obtained and the problems arising from the experimental process in the experimental part of this project will be described and discussed below, and the direct use of the regression algorithm on three different gusts of The shape is analyzed and finally learned to obtain the reconstruction results. The three gust patterns are the '1-cos' gust, the step change gust and the von Kármán gust. The '1-cos' gust and the step change gust are both relatively simple gusts, while the von Kármán shape intersects the first two very complex.

During the experiment, it was found that learning from the global data could not successfully reconstruct the gust, so an experimental scheme for the slicing method of the '1-cos' gust was proposed. Because these gust conditions are not linear problems, and the regression algorithm is mainly suitable for regressing linear changes. Therefore, in the experiment, the data is truncated to ensure that each segment can be successfully learned and reconstructed by the regression algorithm. Relatively speaking, the gust

image and change of the '1-cos' gust are relatively simple, so it is more suitable for regression methods suitable for linear problems.

4.1, Global Learning Using Regression Algorithms

4.1.1, '1-cos' gust

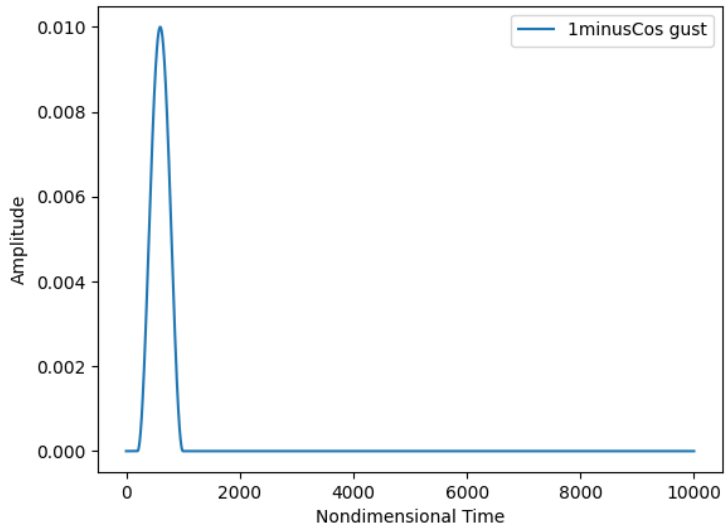

Figure 16. Image of '1-Cos' gust

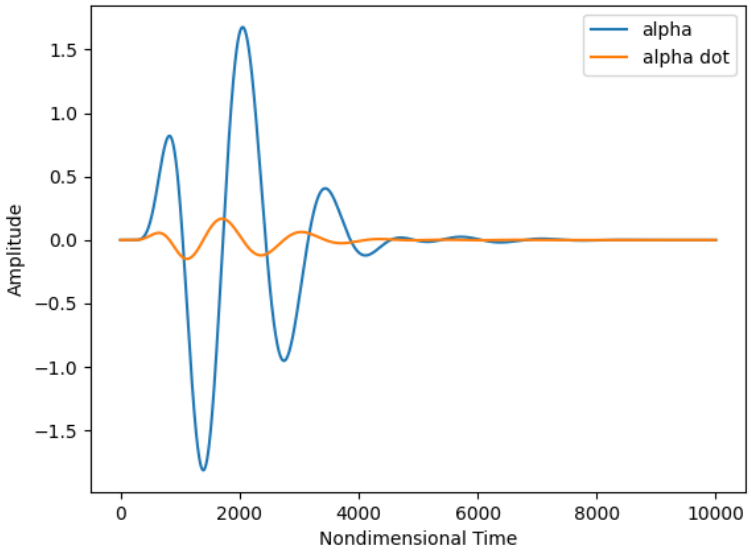

Figure 17. '1-Cos' gust pitch(α) and pitch rate($\dot{\alpha}$)

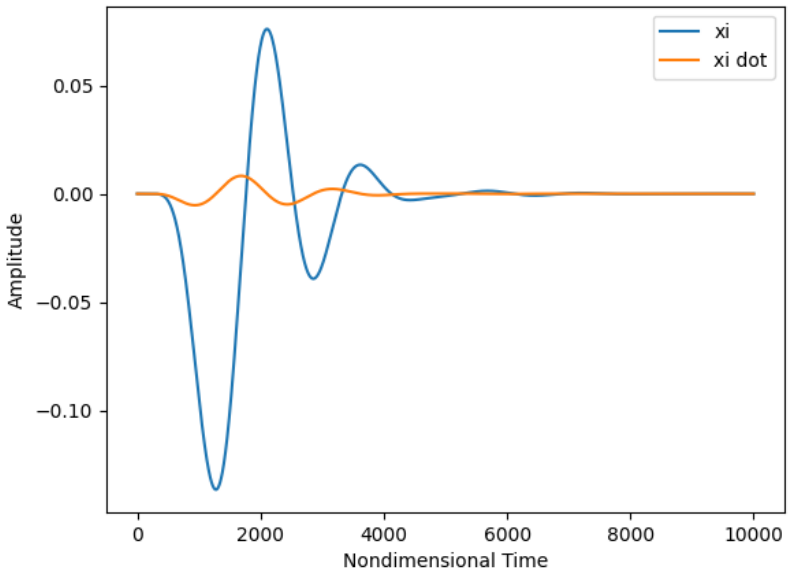

Figure 18. Plunge (ξ) and vertical velocity ($\dot{\xi}$) of '1-Cos' gusts

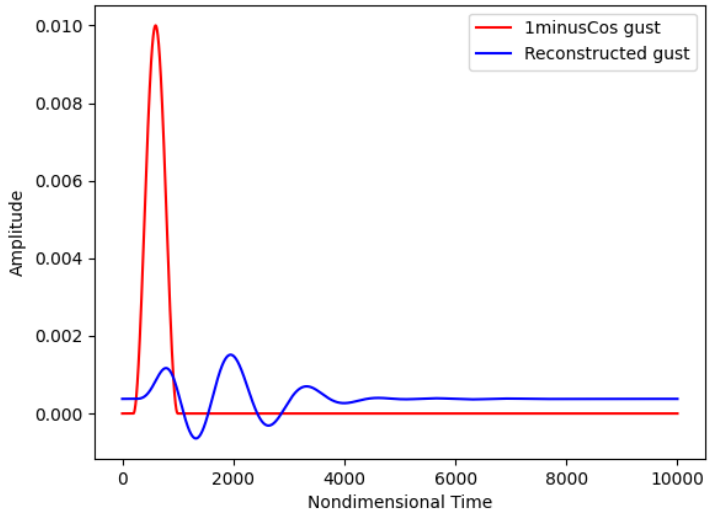

Figure 19. The reconstruction results of machine learning and the image comparison of '1-Cos' gust

4.1.2, step change gust

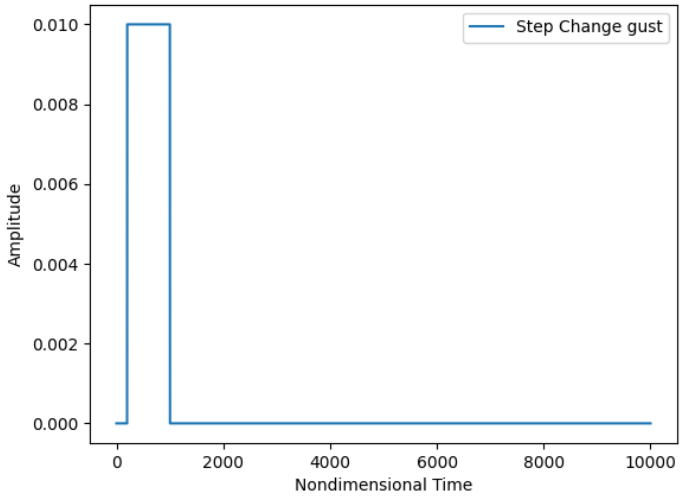

Figure 20. image of step change gust

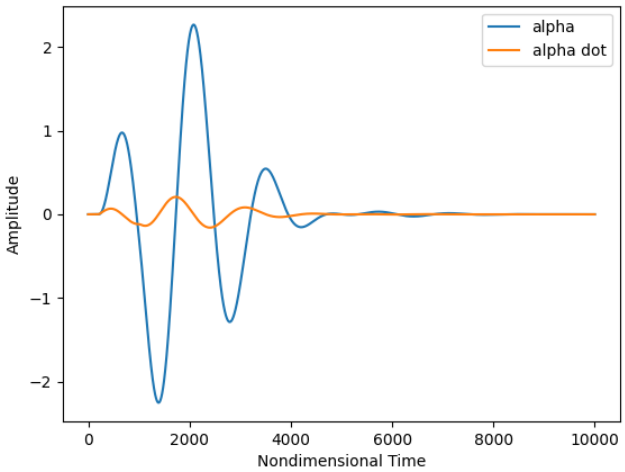

Figure 21. step change gust's pitch(α) and pitch rate($\dot{\alpha}$)

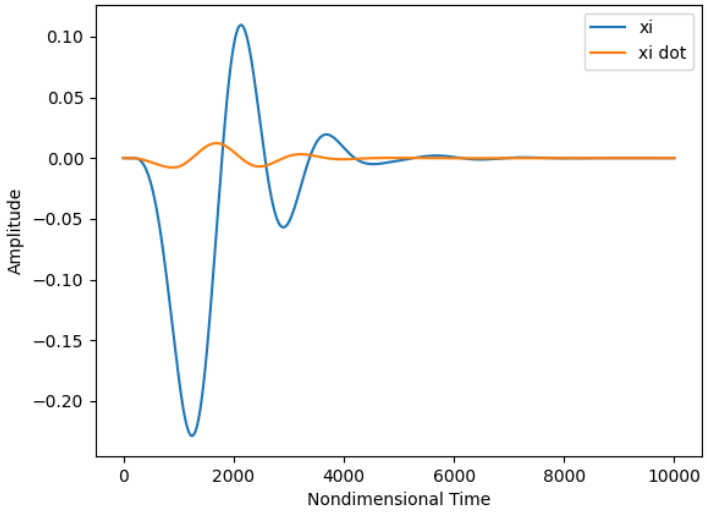

Figure 22. Plunge (ξ) and vertical velocity ($\dot{\xi}$) of step change gust

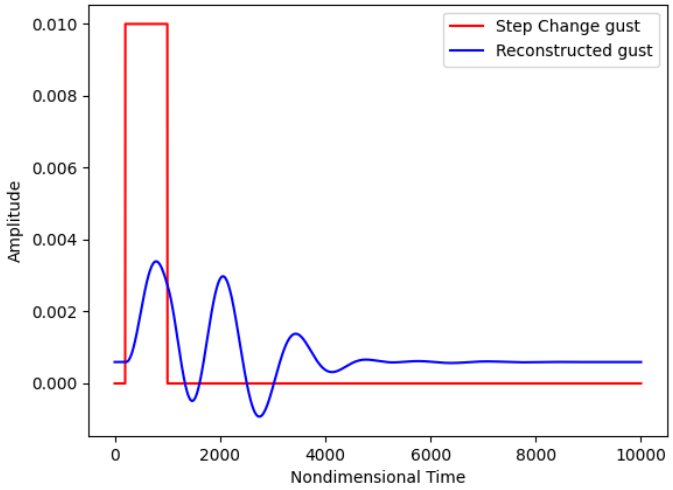

Figure 23. The reconstruction result of machine learning and the image comparison of step change gust

4.1.3, von Kármán gusts

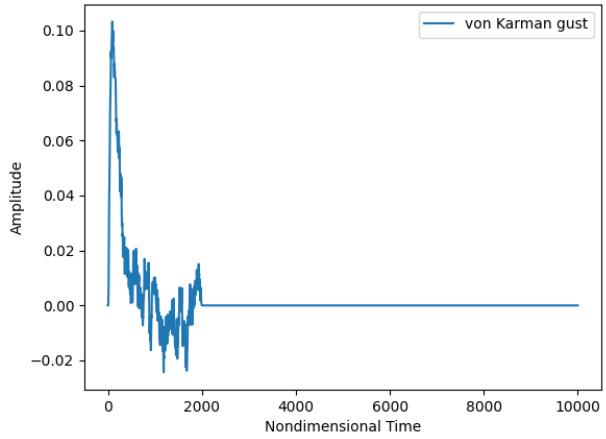

Figure 24. Image of von Kármán gust

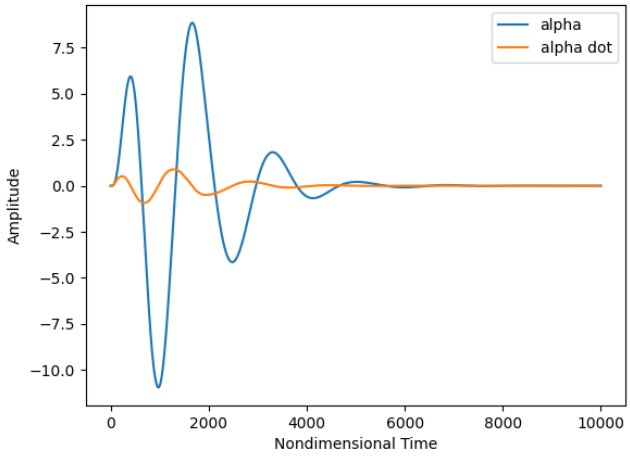

Figure 25. The pitch(α) and pitch rate($\dot{\alpha}$) of the von Kármán gust

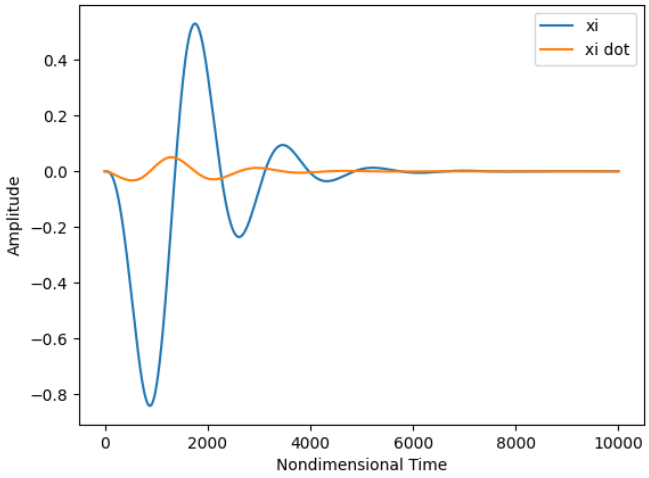

Figure 26. Plunge (ξ) and vertical velocity ($\dot{\xi}$) of von Kármán gusts

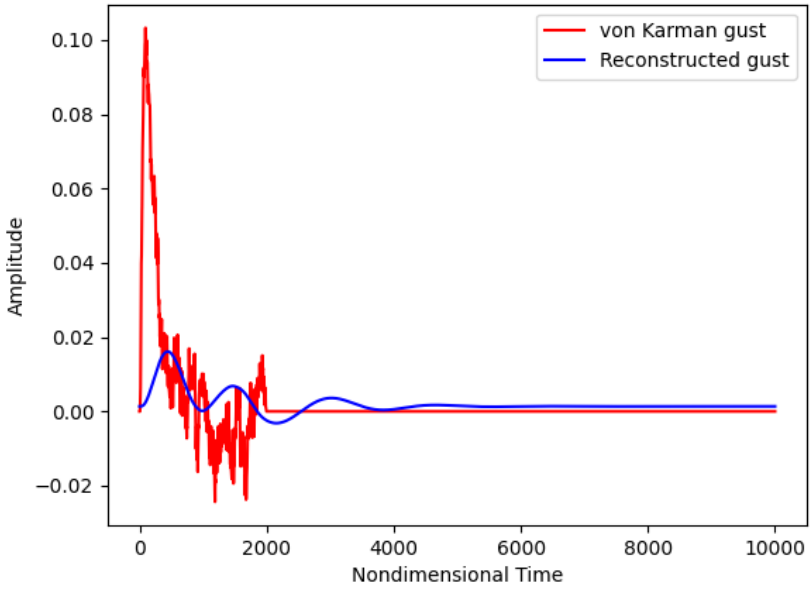

Figure 27. Machine learning reconstruction results and image comparison of von Kármán gust

Summary of Global Learning Using Regression Algorithms

As shown in figure 19, 23 and 27, the results of machine learning can not reconstruct the above three gusts, and in the experiment, it is found that the reconstruction results have no effect on $\vec{w}$ and b in the equation 47 of the above regression algorithm. is very sensitive to changes in , the initial selection of these two variables has a great influence on the reconstruction results, and even an increase or decrease of 0.1 will lead to completely different results. Convergence of the cost function was observed in all reconstructions, so there was no problem with the learning step. On the other hand, because the amount of data is relatively large, the time required for each learning is relatively long. This disadvantage is

especially obvious when setting up random initial $\vec{w}$ and b for many times. If you set 1000 loops and learn 1000 times each time, the time is usually more than 10 minutes. This is also one of the reasons why the method of slicing the data is proposed, because the regression algorithm belongs to supervised learning, and it is very important for the experimenter to adjust and select the starting point data, and if the time cost is too high, the experimental efficiency will be reduced.

4.2, Learning from data slices

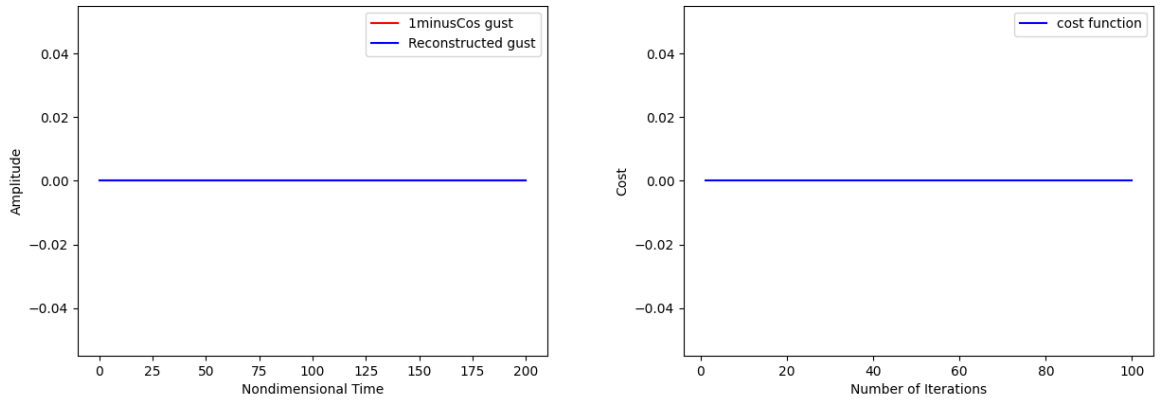

(a) (b)

Figure 28. The reconstruction results of the machine learning of slice segment 1 and the image comparison of the '1-Cos' gust (a) and the cost function during the learning process (b)

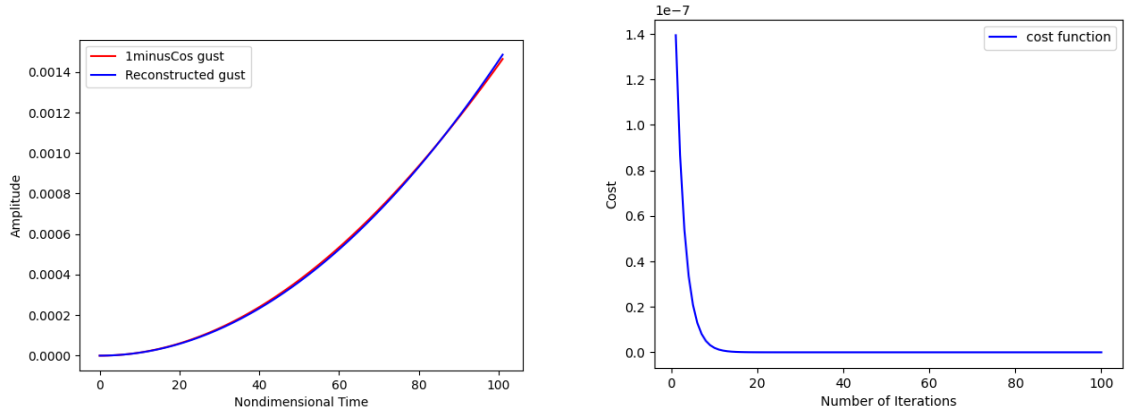

(a) (b)

Figure 29. The reconstruction results of the machine learning of slice segment 2 and the image comparison of the '1-Cos' gust (a) and the cost function during the learning process (b)

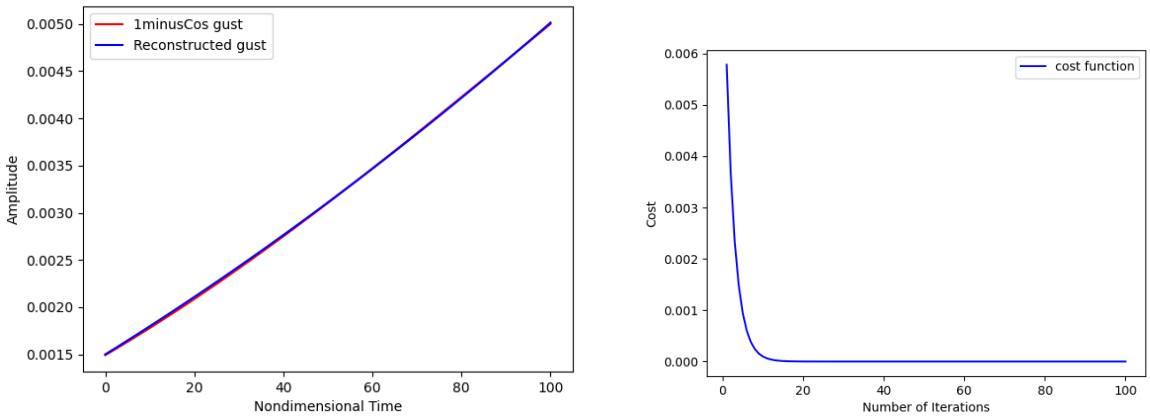

(a) (b)

Figure 30. The reconstruction results of the machine learning of slice segment 3 and the image comparison of the '1-Cos' gust (a) and the cost function during the learning process (b)

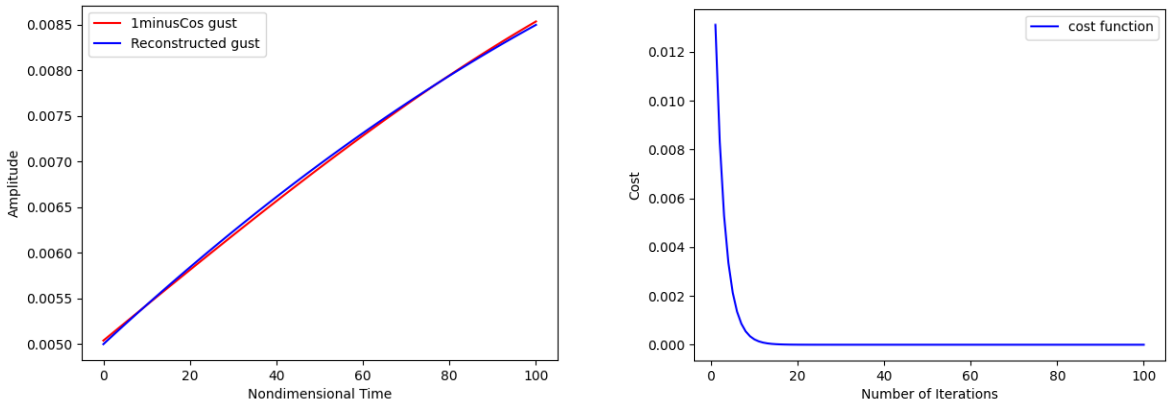

(a) (b)

Figure 31. The reconstruction results of the machine learning of slice segment 4 and the image comparison of the '1-Cos' gust (a) and the cost function during the learning process (b)

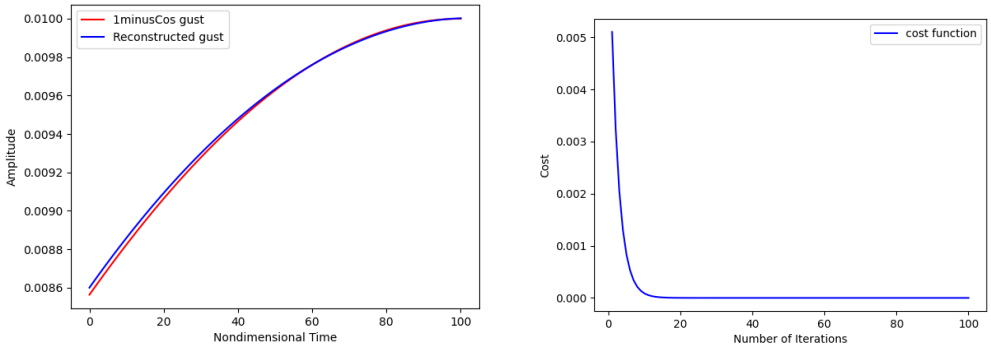

(a) (b)

Figure 32. The reconstruction results of the machine learning of slice segment 5 and the image comparison of the '1-Cos' gust (a) and the cost function during the learning process (b)

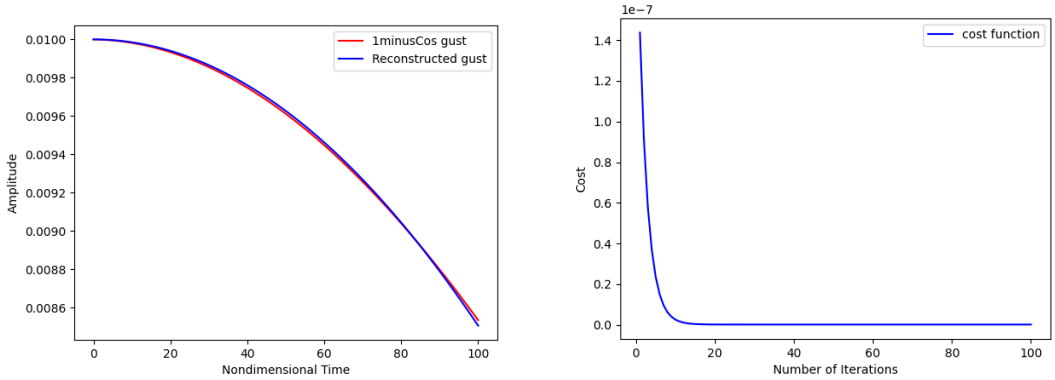

(a) (b)

Figure 33. The reconstruction results of the machine learning of slice segment 6 and the image comparison of the '1-Cos' gust (a) and the cost function during the learning process (b)

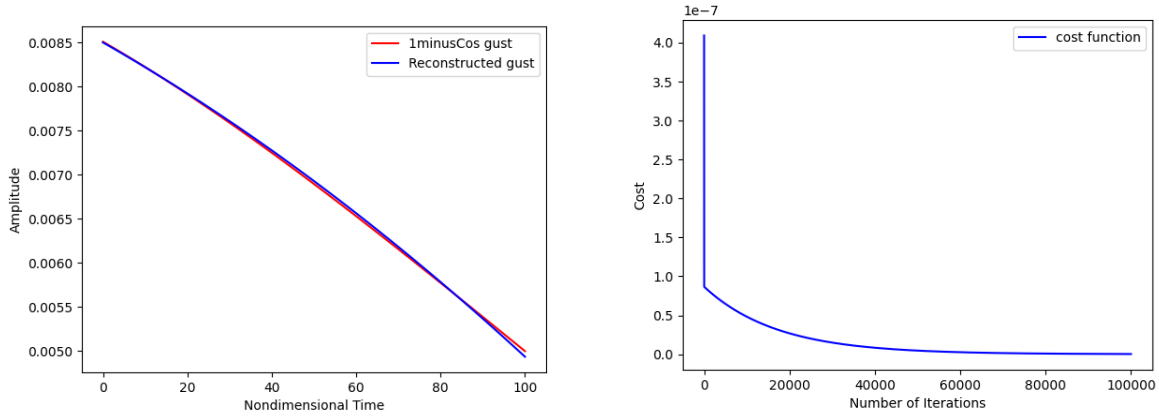

(a) (b)

Figure 34. The reconstruction results of the machine learning of slice segment 7 and the image comparison of the '1-Cos' gust (a) and the cost function during the learning process (b)

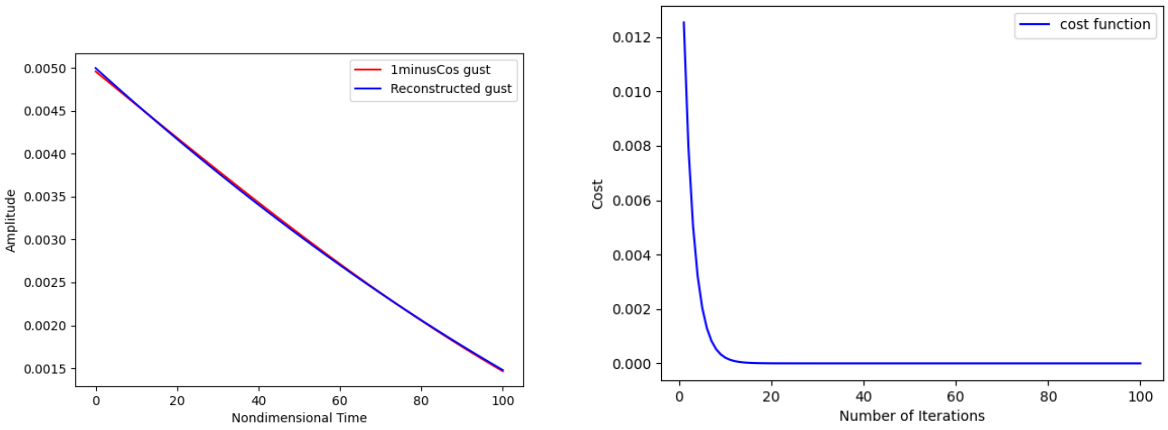

(a) (b)

Figure 35. The reconstruction results of the machine learning of slice segment 8 and the image comparison of the '1-Cos' gust (a) and the cost function during the learning process (b)

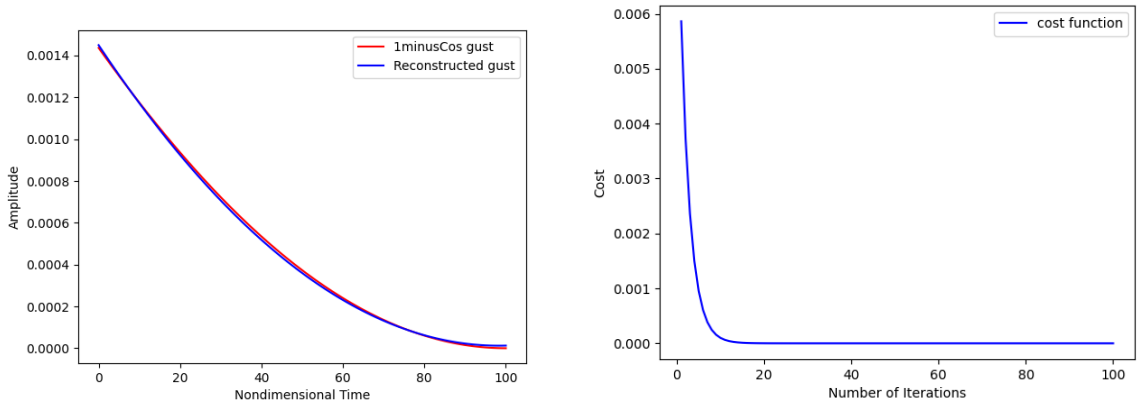

(a) (b)

Figure 36. The reconstruction results of the machine learning of slice segment 9 and the image comparison of the '1-Cos' gust (a) and the cost function during the learning process (b)

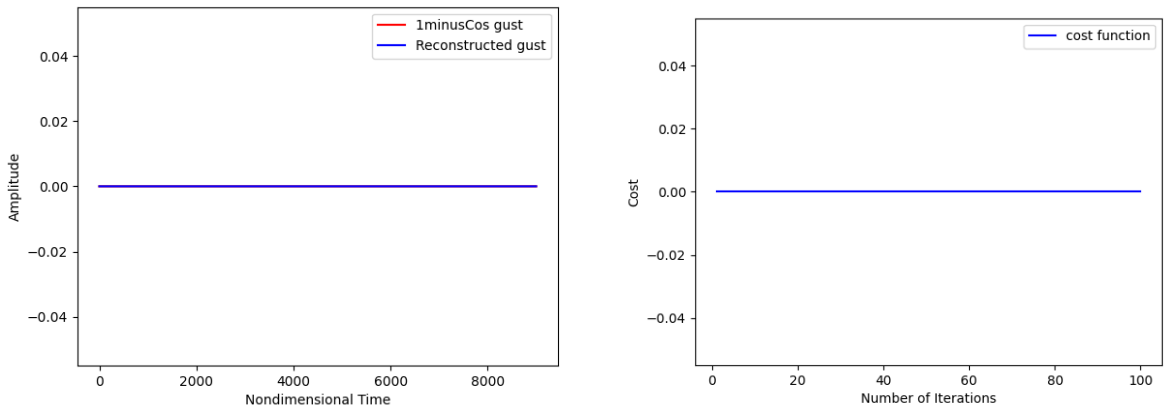

(a) (b)

Figure 37. The reconstruction results of the machine learning of slice segment 10 and the image comparison of the '1-Cos' gust (a) and the cost function during the learning process (b)

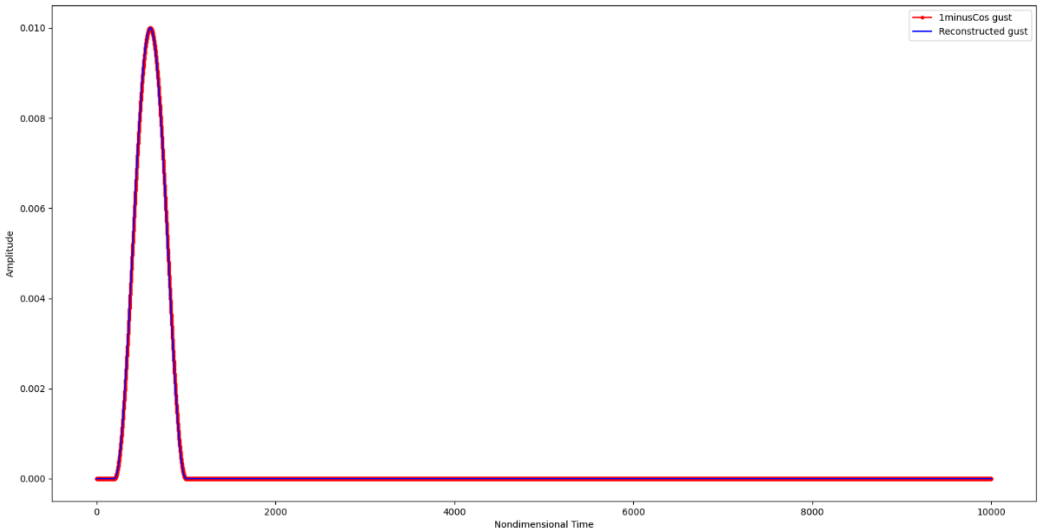

(a)

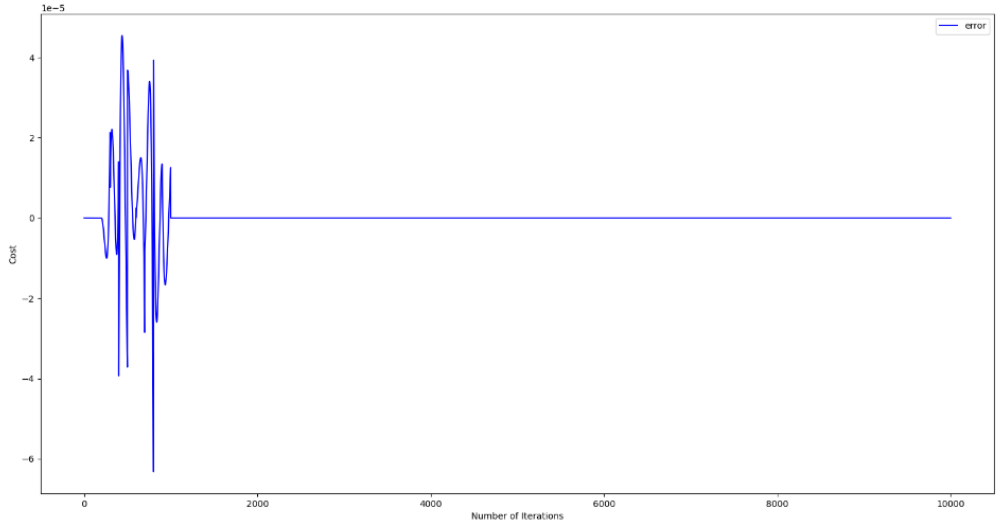

(b)

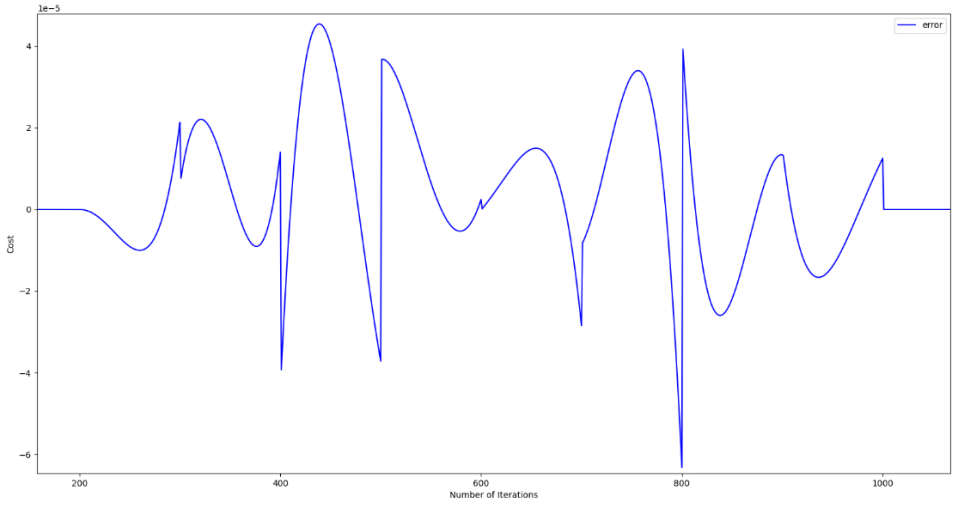

(c)

Figure 38. After splicing the slice fragments, the machine learning reconstruction result and the image comparison of the '1-Cos' gust (a) and the error (b, c)

As shown in the resulting images presented in this section, the accuracy of the gust reconstruction results is significantly improved by slicing the numbers. The final resulting images are also acceptable. But several problems mentioned in the section on global learning using regression algorithm still exist, first of all, it is still quite sensitive to the changes of $\vec{w}$ and b variables in the equation 47 of the regression algorithm, which also leads to the fact that in order to obtain sufficiently accurate results A lot of attempts are required, but compared to learning directly using global data, the time spent on each learning is greatly

shortened due to the small number of data sets. But even so, a lot of time was spent in finding suitable $\vec{w}$ and b in this experiment. Compared with the optimization algorithm, the computational cost increased. The main reason for the increase in computational cost is that the current regression algorithm is suitable for linear problems, and the introduction section also mentioned that, like the inverse method, the linear method does not perform well in nonlinear problems.

In summary, while data slicing enables the regression algorithm to reconstruct simple gusts (such as the '1-Cos' gust), at the same time, as shown in figure 28 and figure 37, in this gust input This method is very efficient for a long time at a constant, because in this case $\vec{w}$ is zero and only b needs to be adjusted. So predictably, for step change gust, it is efficient when using data slicing. However, it is difficult for the regression algorithm to describe the instantaneous gust input change in the step change gust, so when the data slice contains such instantaneous gust input changes, the regression algorithm cannot provide a suitable reconstruction for this data segment.

For the von Kármán gust, its image is too complex and changes so rapidly that regression algorithms struggle to provide accurate results. While it is possible to make the regression algorithm work by slicing small enough, it does not make sense for this study.

5, Discussion

Based on the literature survey included in the introduction section above and the results of the project experiments in the result section, this section will first discuss the current difficulties and reasons for wanting to apply machine learning to gust reconstruction. It also proposes the direction to be explored in the future to reconstruct gusts through machine learning. It will then discuss the regression tree algorithm that was tried but not completed in this experiment, and explain why it is possible to apply the regression tree algorithm to gust reconstruction, why this experiment was not completed, and the difficulties of using this method .

5.1, Gust Reconstruction and Machine Learning

Today, although there are more and more researches on machine learning, generally speaking, it is mainly reflected in the aspect of logical judgment. As mentioned in the introduction, the relevant application research in the aviation field also mainly identifies whether there is damage, which is also a 1 or 0 relationship. Including the two advanced supervised learning methods described in the introduction, in which deep learning can enable machine learning to make judgments of complex problems by increasing the number of layers and the logical judgments included in them, which is also deep learning can be a strong artificial intelligence. Smart reasons. But the essence of deep learning is to simulate the neural network of the human brain. Humans still have not fully determined how the human brain works, so the current deep learning is only a simulation of the working principle of neurons. This also leads to the fact that deep learning is currently mainly used for logical judgment.

The decision tree method mentioned in the introduction is also based on logical judgment. By extracting features to complete classification and logical judgment, this method is widely used in big data analysis and is also very mature in analyzing user preferences and pushing news or products that users may be interested in. But it must be admitted that for the samples contained in leaf nodes, its meaning is also equal to 1 (judgment is yes) or equal to 0 (judgment is no), and decision nodes determine which feature is used to classify the input samples. Most effective here. Although there is also a regression tree algorithm for regression data, it is essentially impossible to change all input features and still can only make judgments of 1 and 0. The regression tree algorithm will be discussed in detail in the next section.

To sum up, at present, in addition to the basic algorithm of the regression algorithm used in this project, most of the other algorithms in machine learning are classified and logically judged, including another basic algorithm, the logistic regression algorithm (this report). not mentioned). Therefore, from the current stage of machine learning development, it is not suitable for complex nonlinear problems such as gust reconstruction that require regression data. But after completing this project, some hypotheses that may in the future enable machine learning to do complex nonlinear problems that require regression data can also be raised.

In deep learning, the essence of each neuron is to build a logistic regression, combine neurons into layers and make complex logical judgments by building multiple layers. So is it possible to give neurons linear regression to complete complex analysis by forming multiple layers, because in this case, more states can be considered through multiple neurons in one layer, by combining these and then by logistic regression Choose the best answer. But this requires a lot of gust data and all the data that might affect the gust response is taken into account as a base, and a lot of trial and learning is done on this basis. In summary, the time cost required to verify this conjecture is enormous.

On the other hand, the linear regression algorithm is currently unable to complete complex data simulation, so in order to make the linear regression method more widely used, you can consider studying the learning function of more complex functions, and how to add restrictions to the regression, such as limiting the maximum value and Values exceeding the maximum value are all equal to the maximum value, etc. Or being able to combine multiple different functions, such as nesting multiple conditions together. These will increase the output of linear regression algorithms and may allow regression algorithms to be applied to nonlinear data regression problems.

5.2, regression tree algorithm

In this experiment, the regression tree method has also been considered, by converting pitch (α), pitch rate ($\dot{\alpha}$), Plunge (ξ) and vertical velocity ($\dot{\xi}$) into features through One-hot encoding , and then each set of data has a feature of 1, and a feature that does not have a feature of 0. The features are classified by regression tree and the gust input corresponding to the feature is finally summarized, so as to complete the reconstruction of the gust load. But there were two main problems that prevented this attempt from being carried out, the computational cost issue and the time issue.

First of all, regarding the computational cost, the von Kármán gust was reclassified and encoded by One-hot encoding. The final result is that there are more than 35,000 different features, and the total amount of this set of von Kármán gust data is 10,001. That is to say, the total amount of data that needs to be classified and judged in the end exceeds 350,035,000, and the files storing these data reach 9.30 GB. Since this project has not applied for any equipment support, this amount of data has basically reached the limit of the hardware used in this study. If this conjecture is to be verified, more advanced device support is required.

On the other hand, the problem of time is also the reason why this study has not continued to explore in this area. Although the data has basically reached the limit of the hardware used in this study, it can still run as long as there is no memory overflow problem. However, because this is just a conjecture, it is necessary to adjust the method after experimental verification to ensure that the results meet the requirements. However, due to the huge amount of data, the current equipment will consume a huge amount of time for a test, which is unacceptable for this project.

However, the regression tree is very effective for summarizing the possible features. If the analysis of the gust data of the regression tree can be completed, the saved data may meet the industrial requirements, and it may also be able to bring some new inspiration for future related research.

Finally, the combination of random forest method and regression tree method can be considered in future research, because the total amount of data is very large, and random forest method can choose to reduce the computational cost required for each decision tree. At the same time, the random forest method will also explore very small changes and average these small changes. This reduces the effects of noise when analyzing experimental data. These properties are beneficial for studying gust reconstruction

6, Conclusion

This experimental project provides a method capable of reconstructing simple nonlinear discrete gusts such as '1-cos' gusts, although the proposed method still requires a lot of time and computation to complete gust simulations and for gusts such as von Kármán gusts Complex Continuous turbulence doesn't work very well. However, based on the results and problems of this project, combined with other machine learning algorithms, the direction of continuing to explore machine learning in the field of gust reconstruction in the future is proposed. As mentioned above, most of the current machine learning research revolves around logical judgment, but there are still viable methods for dealing with complex nonlinear regression problems like gust reconstruction. For improving the efficiency and practicability of machine learning in the field of gust reconstruction, some views and directions based on the problems arising in this project are proposed.

List of Reference

[1] J. Fuller. Evolution and future development of airplane gust loads design requirements. 1997

World Aviation Congress, 32(2):235{246, 1997. ISSN 0021-8669. doi: 10.2514/6.1997-5577.

[2] J. R. Wright and J. E. Cooper. Introduction to Aircraft Aeroelasticity and Loads. Wiley,

2007.

[3] An Introduction to Rigid Aeroplane Response to Gusts and Atmospheric Turbulence.

ESDU 04024, November 2004.

[4] Hubert I. Flomenhoft. Brief history of gust models for aircraft design. Journal of Aircraft,

31(5):1225{1227, 1994. ISSN 0021-8669. doi: 10.2514/3.46637.

[5] Simone Simeone, “Gust Loads Reconstruction for In-Service Support ”, The University of Bristol, 2020

[6] Certification specifications for large aeroplanes. EASA, Amendment 3, September 2003.

[7] Raymond L. Bisplinghoff, Holt Ashley, and Robert L. Halfman. Aeroelasticity. 1983. ISBN

978-0-486-69189-3.

[8] H. Salehi, S. Das, S. Chakrabartty, S. Biswas and R. Burgueño, “Damage identification in aircraft structures with self-powered sensing technology: A machine learning approach ”, Structural Control Health Monitoring, 2018

[9] H. Salehi, S. Das, S. Chakrabartty, S. Biswas and R. Burgueño, “A machine-learning approach for damage detection in aircraft structures using self-powered sensor data”, Proceedings Volume 10168, Sensors and Smart Structures Technologies for Civil, Mechanical, and Aerospace Systems 2017

[10] L. Ai, V. Soltangharaei, M. Bayat, M. Tooren and P. Ziehl, “ Detection of impact on aircraft composite structure using machine learning techniques”, Measurement Science and Technology, 2021

[11] T. Theodorsen. General theory of aerodynamic instability and the mechanism of utter.

Technical report, 1935.

[12] A. Da Ronch, K. Badcock, Y.Wang, A. Wynn, and R. Palacios. Nonlinear Model Reduction

for Flexible Aircraft Control Design. AIAA Atmospheric Flight Mechanics Conference,

pages 1{23, 2012. doi: 10.2514/6.2012-4404. URL http://arc.aiaa.org/doi/abs/10.

2514/6.2012-4404.

[13] L. Meirovitch. Dynamics and Control of Structures. Wiley, New York, 1989.

[14] S. Simeone, C. Agostinelli, T. Rendall and A. Rampurawala, “Gust Reconstruction from Digital Flight Data Recorder via Numerical Optimisation" in 57h AIAA/ASCE/AHS/ASC Structures, Structural Dynamics, and Materials Conference, San Diego, California, 2016.

[15] S. Simeone, T. Rendall, A. Da Ronch and A. Rampurawala, “A Gust Reconstruction Framework Applied to a Nonlinear Reduced Order Model of a Wing Typical Section" in 58h AIAA/ASCE/AHS/ASC Structures, Structural Dynamics, and Materials Conference, Grapevine, Texas, 2017.

[16] S. Simeone, T. Rendall, S. Williams, C. W.Wales, J. Cooper, D. Jones and A. L. Gaitonde, “Reconstruction of Gust Velocity Profiles via Potential Flow, CFD and ROM techniques" in International Forum for Aeroelasticity and Structural Dynamics, Como, Italy, 2017.

[17] S. Simeone, \Problem Structuring Methods applied to define In-Service Support Development in a Large Aircraft Manufacturer" submitted to the University of Bristol as a requirement of the Socio Technical Systems module, EngD Programme, Bristol, UK, 2014.

[18] S. Simeone, “A Systems Engineering Approach for Information Systems Development in a Large Aircraft Manufacturer" submitted to the University of Bristol as a requirement of the Systems Engineering module, EngD Programme, Bristol, UK, 2014.

Appendix 1

Gust-Related Derivatives [1]

$$Z_{gW} = -\frac{1}{2}\rho V S_W a_W \quad and \quad Z_{gT} = -\frac{1}{2}\rho V S_T a_T (1 - k_\epsilon)$$

$$M_{gW} = -\frac{1}{2}\rho V S_W a_W l_W \quad and \quad Z_{gT} = -\frac{1}{2}\rho V S_T a_T l_T (1 - k_\epsilon)$$